nature medicine

ARTICLES

https://doi.org/10.1038/s41591-018-0217-1

Translational control of tumor immune escape via the eIF4F–STAT1–PD-L1 axis in melanoma

Michaël Cerezo[1,2,12], Ramdane Guemiri[1,2,3,4,5,12], Sabine Druillennec[5,6,7], Isabelle Girault[1,2], Hélène Malka-Mahieu[3,4,5], Shensi Shen[1,2], Delphine Allard[1,2], Sylvain Martineau[3,4,5], Caroline Welsch[1,2,3,4,5], Sandrine Agoussi[1,2], Charlène Estrada[5,6,7], Julien Adam[1,8], Cristina Libenciuc[9], Emilie Routier[9], Séverine Roy[9], Laurent Désaubry[10], Alexander M. Eggermont[2,9], Nahum Sonenberg[11], Jean Yves Scoazec[8], Alain Eychène[5,6,7], Stéphan Vagner[3,4,5,9,13*] and Caroline Robert[1,2,9,13*]

Preventing the immune escape of tumor cells by blocking inhibitory checkpoints, such as the interaction between programmed death ligand-1 (PD-L1) and programmed death-1 (PD-1) receptor, is a powerful anticancer approach. However, many patients do not respond to checkpoint blockade. Tumor PD-L1 expression is a potential efficacy biomarker, but the complex mechanisms underlying its regulation are not completely understood. Here, we show that the eukaryotic translation initiation complex, eIF4F, which binds the 5′ cap of mRNAs, regulates the surface expression of interferon-γ-induced PD-L1 on cancer cells by regulating translation of the mRNA encoding the signal transducer and activator of transcription 1 (STAT1) transcription factor. eIF4F complex formation correlates with response to immunotherapy in human melanoma. Pharmacological inhibition of eIF4A, the RNA helicase component of eIF4F, elicits powerful antitumor immune-mediated effects via PD-L1 downregulation. Thus, eIF4A inhibitors, in development as anticancer drugs, may also act as cancer immunotherapies.

Immune checkpoint blockade was first explored in patients with metastatic melanoma, where it translated into clinical benefit with the use of anti-CTLA4 antibody (ipilimumab)[1,2], which was rapidly surpassed by the more effective and less toxic anti-PD-1 antibodies (pembrolizumab and nivolumab)[3,4]. This concept has radically modified cancer management worldwide, and within only a few years anti-PD-1 or anti-PD-L1 antibodies have been approved in several other cancers, including lung, renal cell and Hodgkin lymphoma, and are presently being evaluated in almost all types of cancers[5]. In spite of these major steps forward, primary or secondary resistance to immunotherapy occurs for the majority of patients, and reliable and dynamic predictive biomarkers are still needed.

The rationale for the use of anti-PD-1 or anti-PD-L1 antibodies is that interferon-γ (IFN-γ) secreted by metastases-infiltrating lymphocytes will eventually lead to tumor evasion by upregulating negative immune checkpoints such as PD-L1 (ref. [6]). However, PD-L1 expression is regulated in tumors in several different ways, in addition to being induced by IFN-γ secreted by infiltrating lymphocytes as a mechanism of immune escape[6]. It may be constitutively expressed due to genetic PD-L1 locus amplification[7]. PD-L1 regulation has also been described at the transcriptional and RNA stability levels by MYC and oncogenic RAS, respectively[8,9], as well as at the protein level by the CSN5, CMTM4 and CMTM6 proteins[10–12]. Notably, the regulation of PD-L1 expression by MYC, RAS, CSN5 or CMTM4/6 has been studied independently of the presence of surrounding T lymphocytes and of the effect of IFN-γ. In the absence of the T cell environment, however, tumor cell–intrinsic PD-L1 expression is not typically associated with the response to immunotherapy. This explains why PD-L1 expression alone is not a strong predictive biological marker of PD-1 blockade efficacy[13].

In addition to gene expression regulation at the transcriptional and post-translational levels, the translational control of gene expression is increasingly considered a critical effector in cancer biology[14–18]. More specifically, the essential eIF4F eukaryotic translation initiation complex (consisting of eIF4A, eIF4E and eIF4G), which binds to the 7-methylguanylate cap at the 5′ end of all mRNA and sustains protein synthesis, has been implicated in the etiology of many human cancers[16]. Owing to its location downstream of many oncogenic signaling networks, including the PI3K–mTOR and RAS–MAPK (mitogen-activated protein kinase) pathways, eIF4F complex formation is associated with resistance to anticancer agents such as HER2, BRAF and MEK inhibitors in a variety of cancers[19,20]. The eIF4G scaffolding protein interacts with both 40S ribosome–associated factors and the eIF4E cap-binding protein to recruit the 40S ribosome to the cap. Recruitment of 40S to mRNAs is dependent on cap accessibility and on the level of RNA secondary structure present in the vicinity of the cap, which is controlled by the RNA unwinding activity of the eIF4A RNA helicase. eIF4F activity is not an 'all or nothing' translation checkpoint but has distinct requirements on the helicase activity of eIF4A toward different mRNAs with various levels of secondary structure in their 5′ untranslated regions (5′ UTR)[21], resulting

[1]INSERM U981, Gustave Roussy, Villejuif, France. [2]Université Paris Sud, Université Paris-Saclay, Kremlin-Bicêtre, France. [3]Institut Curie, PSL Research University, CNRS UMR 3348, Orsay, France. [4]Université Paris Sud, Université Paris-Saclay, CNRS UMR 3348, Orsay, France. [5]Equipe Labellisée Ligue Contre le Cancer, Paris, France. [6]Institut Curie, PSL Research University, CNRS UMR 3347, INSERM U1021, Orsay, France. [7]Université Paris Sud, Université Paris-Saclay, CNRS UMR 3347, INSERM U1021, Orsay, France. [8]Department of Pathology and Laboratory Medicine (BIOpath), Gustave Roussy, Univesité Paris-Saclay, Villejuif, France. [9]Oncology Department, Gustave Roussy, Université Paris-Saclay, Villejuif, France. [10]CNRS-Strasbourg University, UMR7200, Illkirch, France. [11]Department of Biochemistry, McGill University, Montréal, Québec, Canada. [12]These authors contributed equally: Michaël Cerezo, Ramdane Guemiri. [13]These authors jointly supervised this work: Stéphan Vagner, Caroline Robert. *e-mail: stephan.vagner@curie.fr; caroline.robert@gustaveroussy.fr

in highly variable translation initiation rates and selective mRNA translation control.

The levels of the individual components of the eIF4F complex, and its activity, are elevated in many human cancers, constituting vulnerability for transformed cells. In addition small molecule inhibitors of eIF4F exert potent antitumor effects, offering an opportunity for therapeutic intervention[16,22–24]. Therefore, we investigated the role of eIF4F on the mechanisms of immune escape by tumor cells, and more specifically on the regulation of T lymphocyte–induced PD-L1 expression.

Results

eIF4F inhibition blocks PD-L1 induction in cancer cells. To study the role of the eIF4F complex in PD-L1 expression induced in response to the T cell environment, we first used IFN-γ-treated melanoma cell lines, as they tend to have a lower basal PD-L1 expression (mRNA levels) than most other tested tumor cell lines[25] (Supplementary Fig. 1a) and PD-L1 surface expression can be efficiently and dose-dependently induced by IFN-γ (Supplementary Fig. 1b). eIF4F inhibition was achieved by using either siRNAs targeting each of the individual components of the eIF4F complex or specific eIF4A small-molecule inhibitors (eIF4Ai). Silvestrol, one of the most potent and specific eIF4A inhibitors[26,27], decreases eIF4A levels[28], exhibits antitumor activity[20,28,29] and exerts its effects by selectively inhibiting the translation of key oncogenic mRNAs[21,29,30].

siRNA-mediated depletion of the three individual components of the eIF4F complex (that is, eIF4A, eIF4E or eIF4G), using two different siRNAs targeting each component, significantly decreased expression of IFN-γ-induced PD-L1 surface expression in the BRAF-V600E-mutated A375 and NRAS-Q61R-mutated SKMel10 melanoma cell lines (Fig. 1a and Supplementary Fig. 1c).

Silvestrol led to a decrease in IFN-γ-induced PD-L1 surface expression induced by either IFN-γ (Fig. 1b) or conditioned medium of human activated lymphocytes (Fig. 1c). Silvestrol had no effect on PD-L1 surface expression in WM793 (Fig. 1b), one of the few melanoma cell lines expressing high levels of PD-L1, even in the absence of IFN-γ (Supplementary Fig. 1d). This indicates that eIF4A inhibition is restricted to IFN-γ-induced PD-L1 surface expression. The inhibitory effect of silvestrol on IFN-γ-induced PD-L1 surface expression was also observed in a variety of melanoma, breast and colon tumor cell lines (Fig. 1d–g). The specificity of the effects observed on silvestrol treatment was ascertained by using A375 cells that were rendered resistant to silvestrol (A375-SR) (Supplementary Fig. 2a) and exhibited decreased eIF4F formation (Supplementary Fig. 2b) and cap-dependent mRNA translation (Supplementary Fig. 2c). Silvestrol was not able to decrease IFN-γ-induced PD-L1 surface expression in A375-SR cells (Supplementary Fig. 2d). In addition, other small molecules targeting eIF4A but acting through different mechanisms of action, such as flavagline (FL3) (a synthetic silvestrol derivative[20]), hippuristanol (which allosterically inhibits the binding of mRNA to eIF4A[31]) and pateamine A (which prevents eIF4A binding to eIF4G[32]), also led to a decrease in PD-L1 surface expression (Fig. 1g).

Collectively, these data demonstrate that genetic as well as pharmacological eIF4A inhibition decreases IFN-γ-inducible PD-L1 expression in a variety of tumor cellular cell lines.

An increase in eIF4F complex formation is associated with enhanced IFN-γ-induced PD-L1 surface expression. To further explore the association between eIF4F and IFN-γ-induced PD-L1 surface expression in melanoma, we used murine cell lines derived from melanoma tumors obtained in a mouse model. These mice were genetically engineered (Supplementary Fig. 3a,b) from crossing (i) *Braf*$^{+/LSL\text{-}V600E}$;*Tyr*::*CreERT2*$^{o/o}$ mice, which recapitulate human BRAF-V600E-induced melanoma by inducing BRAF-V600E expression in melanocytes[33], with (ii) *4ebp1*$^{-/-}$;*4ebp2*$^{-/-}$ double-knockout mice that do not express 4E binding proteins 1 and 2 (4E-BP1 and 4E-BP2), which are inhibitors of eIF4F complex formation[34]. To monitor eIF4F complex formation, we used a proximity ligation assay (PLA), which constitutes a sensitive tool for examining protein–protein interactions in cells, to visualize the interaction between eIF4E and eIF4G[20] (Supplementary Fig. 3c). We observed an increase in eIF4F complex formation (eIF4E–eIF4G interaction; red dots)[20] in the *Braf*^{V600E}*4ebp1*$^{-/-}$*4ebp2*$^{-/-}$ cell lines compared with the *Braf*^{V600E} cell lines (Fig. 2a,b) The specificity of the eIF4E–eIF4G PLA was evaluated by using a siRNA against *Eif4e* and by omitting the primary antibodies[20] (Supplementary Fig. 3d). Although constitutive PD-L1 surface expression is low in these cell lines, IFN-γ-stimulated PD-L1 surface expression more efficiently in the *Braf*^{V600E}*4ebp1*$^{-/-}$*4ebp2*$^{-/-}$ cell lines than in the *Braf*^{V600E} cell lines (Fig. 2c). Consistently, the surface expression of PD-L1 was higher in the *Braf*^{V600E}*4ebp1*$^{-/-}$*4ebp2*$^{-/-}$ allografted tumors than in the *Braf*^{V600E} allografts grown in nonmodified C57BL/6 mice (Fig. 2d). Considering that 4E-BP1 and 4E-BP2 were previously reported to be negative regulators of type-I IFN production via translational repression of the mRNA encoding interferon regulatory factor 7 (IRF7)[35], we monitored PD-L1 surface expression following IRF7 silencing and IFN-β or IFN-γ treatment in *Braf*^{V600E} and *Braf*^{V600E}*4ebp1*$^{-/-}$*4ebp2*$^{-/-}$ melanoma cell lines. Compared with IFN-β, IFN-γ induced higher PD-L1 surface expression and IRF7 silencing had no effect on PD-L1 induction (Supplementary Fig. 4), ruling out involvement of the type-I IFN–IRF7 pathway in PD-L1 expression.

Thus, an increase in eIF4F complex formation is associated with enhanced IFN-γ-induced PD-L1 surface expression in murine tumor cell lines and tumors.

eIF4F formation is correlated with inducible PD-L1 expression in melanoma patient samples. To extend our conclusions to human tumors, we analyzed paraffin-embedded formalin-fixed baseline tumor samples from a cohort of 59 patients with metastatic melanoma treated with the anti-PD-1 monoclonal antibody pembrolizumab. We used in situ PLA to assess eIF4F complex formation[20] and immunohistochemistry (IHC) to assess PD-L1 and CD8 expression in tumor biopsies (Fig. 3a). Of note, PD-L1 can be expressed independently of tumor-infiltrating activated lymphocytes via various alternative tumor cell–intrinsic mechanisms, partly explaining why PD-L1 expression level determined by IHC represents a mediocre indicator of response to anti-PD-1 (ref. [13]) (Supplementary Fig. 5a,b). Thus, to identify tumor samples in which PD-L1 expression is induced by infiltrating T cells, we monitored the presence of CD8-positive T cells by IHC. We found a significant correlation between PD-L1 expression and CD8-positive T cell density (Fig. 3b), as well as eIF4F complex formation (Fig. 3c and Supplementary Fig. 5b). This suggests that eIF4F complex formation is correlated with inducible PD-L1 expression in human samples. As expected from these results, a significant correlation ($P=0.0035$) was observed between the clinical response to anti-PD-1 treatment and the activation status of the eIF4F complex (Fig. 3d). The specificity of the eIF4E–eIF4G PLA in patient samples was evaluated by omitting the primary antibodies (Supplementary Fig. 5c). We also set up a PLA approach to explore the proximity between PD-1 and PD-L1 in tumors from patients (Fig. 3e), which is representative of induced PD-L1 expression in the presence of CD8-positive T cells. The specificity of the PLA for PD-1–PD-L1 was evaluated in comparison with PD-1 and PD-L1 IHC on lymph node and tumor samples (Supplementary Fig. 6). We found that eIF4F complex formation (determined by PLA) is significantly correlated ($P=0.0168$) with PD-1–PD-L1 engagement (Fig. 3f).

Altogether, the data obtained on human tumor samples indicate that eIF4F complex formation is associated with inducible PD-L1 expression in patient samples. It also suggests that eIF4F complex

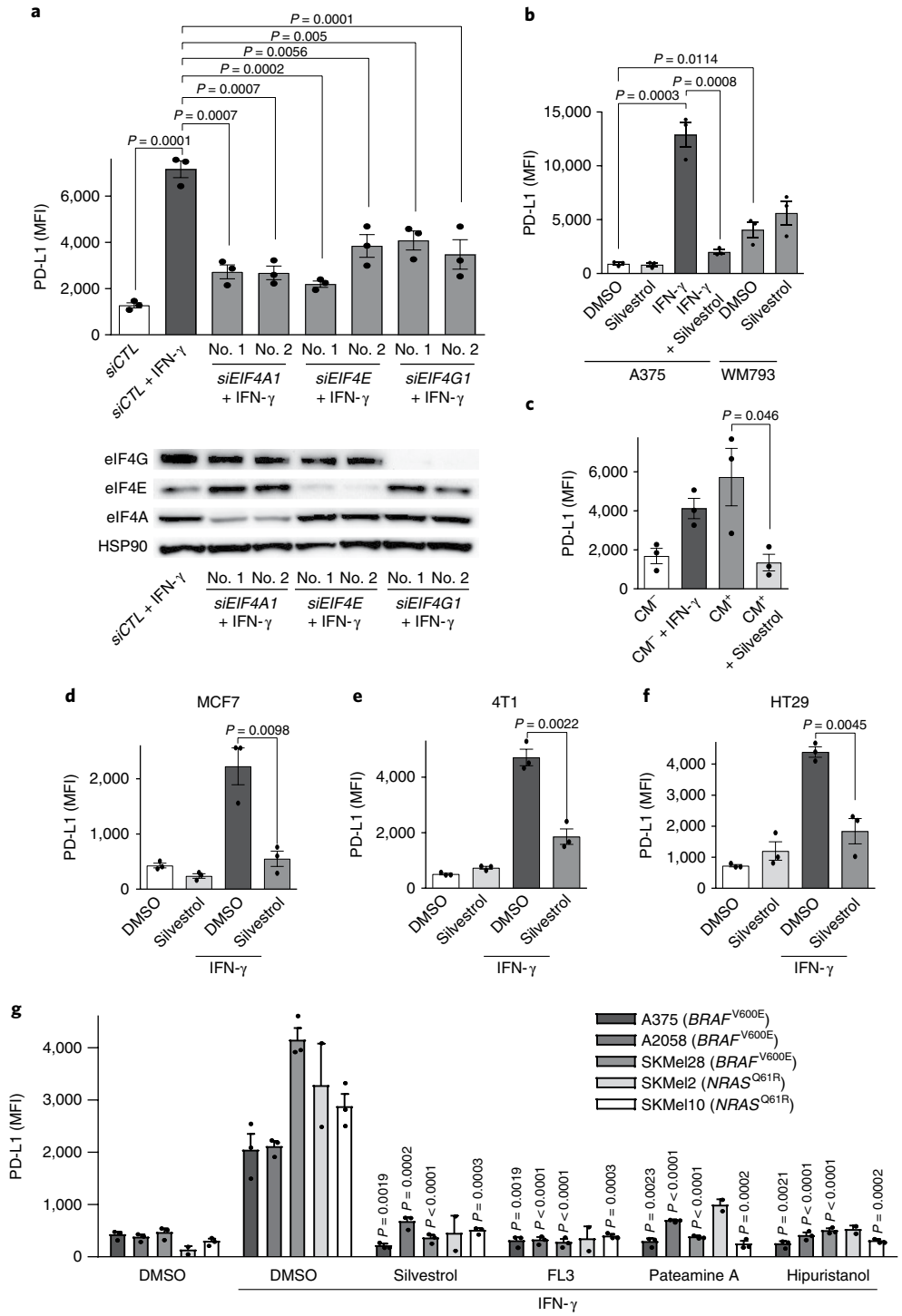

Fig. 1 | eIF4F inhibition blocks PD-L1 induction in cancer cells. a, Top, PD-L1 mean fluorescence intensity (MFI) of A375 cells transfected with the indicated siRNAs (two per gene) and treated with IFN-γ. The data are presented as the mean ± s.e.m. ($n = 3$ independent experiments). *P* values were calculated using two-tailed unpaired *t*-test. Bottom, Western blot analysis of the indicated proteins. **b**, PD-L1 was visualized by flow cytometry in A375 and WM793 melanoma cells treated with IFN-γ (200 ng ml^{-1}) and silvestrol (30 nM). The data are presented as the mean ± s.e.m. ($n = 3$ independent experiments). *P* values were calculated using two-tailed unpaired *t*-test. **c**, PD-L1 MFI in A375 melanoma cells treated with IFN-γ (200 ng ml^{-1}), silvestrol (30 nM), or conditioned medium from activated (CM^+) or nonactivated (CM^-) lymphocytes. The data are presented as the mean ± s.e.m. ($n = 3$ independent experiments). *P* values were calculated using two-tailed unpaired *t*-test. **d**–**f**, PD-L1 visualized by flow cytometry using MCF7 (**d**), 4T1 (**e**) and HT29 (**f**) cells treated with silvestrol (30 nM) and IFN-γ (200 ng ml^{-1}). The data are presented as the MFI of PD-L1 ± s.e.m. ($n = 3$ independent experiments). *P* values were calculated using two-tailed unpaired *t*-test. **g**, Melanoma cells were treated with silvestrol (30 nM), FL3 (10 nM), pateamine A (10 μM), hipuristanol (1 μM) and IFN-γ (200 ng ml^{-1}), and PD-L1 was visualized by flow cytometry. The data are presented as the MFI of PD-L1 ± s.e.m. (A375, A2058, SKMel28, SKMel10 $n = 3$ and SKMel2 $n = 2$ independent experiments). *P* values were calculated using two-tailed unpaired *t*-test.

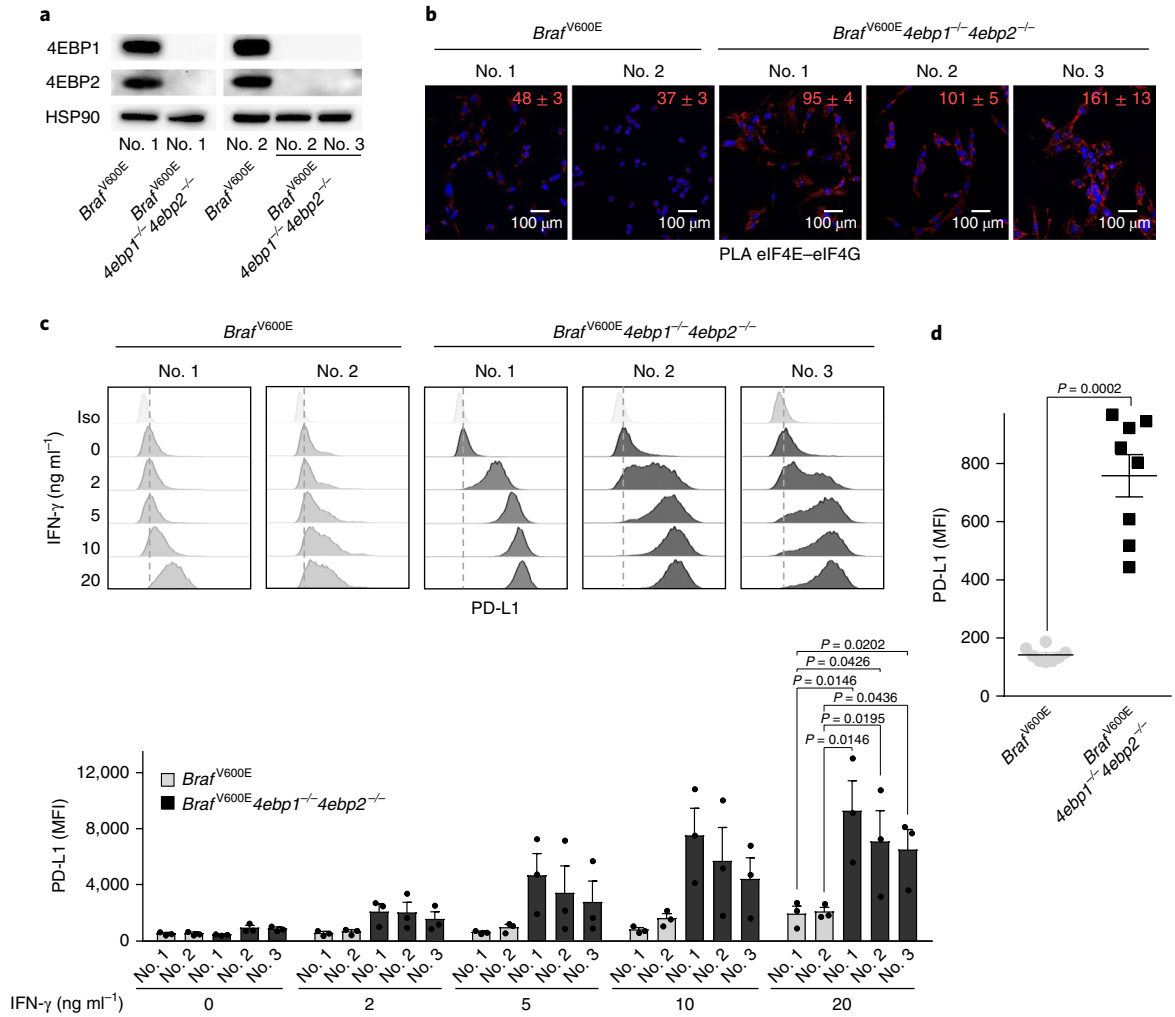

Fig. 2 | eIF4F stimulation increases PD-L1 induction in melanoma cells. a, Western blot analysis of the indicated proteins in *Braf*^{V600E} and *Braf*^{V600E}*4ebp1*$^{-/-}$*4ebp2*$^{-/-}$ murine melanoma cell lines. Representative blots from two independent experiments are shown. **b**, PLA between eIF4E and eIF4G in *Braf*^{V600E} and *Braf*^{V600E}*4ebp1*$^{-/-}$*4ebp2*$^{-/-}$ murine melanoma cell lines. The number of PLA spots per cell ± s.e.m. is indicated in red (*Braf*^{V600E}, no. 1 $n=11$ no. 2 $n=14$; *Braf*^{V600E}*4ebp1*$^{-/-}$*4ebp2*$^{-/-}$, no. 1 $n=11$, no. 2 $n=12$, no. 3 $n=14$ fields). Representative PLA from two independent experiments are shown. **c**, PD-L1 MFI in IFN-γ-treated *Braf*^{V600E} and *Braf*^{V600E} *4ebp1*$^{-/-}$*4ebp2*$^{-/-}$ murine melanoma cell lines. Representative profiles of three independent experiments (top) and MFI PD-L1 of the three experiments (bottom) are shown. The data are presented as the mean ± s.e.m. ($n=3$ independent experiments). *P* values were calculated using one-tailed unpaired *t*-test. **d**, PD-L1 MFI measured in *Braf*^{V600E} and *Braf*^{V600E}*4ebp1*$^{-/-}$*4ebp2*$^{-/-}$ dissociated tumors established after subcutaneously injecting the corresponding cell lines into C57BL/6 mice. The data are presented as the mean ± s.e.m. *P* values were calculated using two-tailed Mann–Whitney test ($n=8$ tumors per group).

formation could be a new biomarker for the response to anti-PD-1 blockade. This is illustrated in the present patient cohort, where, although most of the good responders to anti-PD-1 treatment had a tendency to exhibit elevated expression of PD-L1, the correlation was decreased because two discordant samples in the nonresponding set exhibited high PD-L1 expression but no CD8-positive T cell infiltrates (Supplementary Fig. 5a,b). In these samples, PD-L1 was expressed at a high level independently of the CD8-positive T cell environment; this might explain why the tumor did not respond to treatment. By contrast, the eIF4F PLA signal was very weak in the samples from these patients.

eIF4F regulates the translation of *STAT1* mRNA. We next sought to unravel the mechanism underlying the link between eIF4F complex formation and inducible PD-L1 surface expression observed both in vitro and in vivo. We initially hypothesized that the translation of the mRNA encoding PD-L1 was regulated by eIF4F. However, we found that the level of the *PD-L1* mRNA was strongly decreased by eIF4A inhibition, according to qRT–PCR analysis in two different melanoma cell lines (Fig. 4a and Supplementary Fig. 7a,b). Notably, the decrease in the *PD-L1* mRNA began 8 h after the addition of silvestrol and reached a maximum at 24 h (Fig. 4b). This result reflected a transcriptional effect, as opposed to a translational effect, since the inhibition of eIF4A also reduced luciferase expression driven by the *PD-L1* promoter (Fig. 4c and Supplementary Fig. 7c,d). Of note, in INF-γ-untreated cells, *PD-L1* mRNA levels are regulated by the c-Myc transcriptional regulator[8]. Considering that expression of c-Myc is known to be regulated by eIF4F[36], we analyzed the role of c-Myc in INF-γ-stimulated cells. siRNA-mediated silencing of c-Myc had no effect on PD-L1 surface expression, showing that c-Myc is not involved in IFN-γ-dependent PD-L1 induction (Supplementary Fig. 8).

Therefore, we hypothesized that silvestrol might first inhibit the translation of mRNAs encoding proteins activating IFN-γ-induced PD-L1 transcription, thereby leading to a delayed decrease in *PD-L1* mRNA levels. To obtain a global view of the silvestrol-dependent

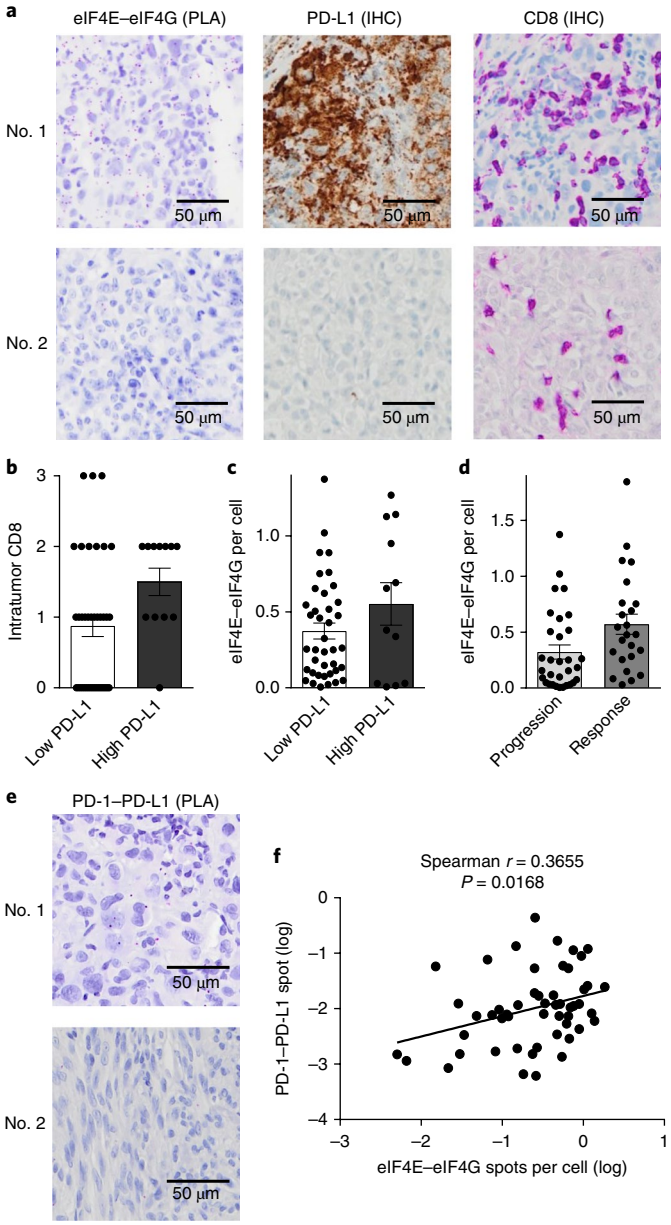

Fig. 3 | eIF4F complex formation is correlated with inducible PD-L1 expression in melanoma patient samples. a, PLA of eIF4E–eIF4G and immunohistochemistry (IHC) of PD-L1 and CD8 are shown for 2 representative tumors from a total of 59 (patient no. 1, who is a responder to anti-PD1 therapy and patient no. 2, who did not respond to anti-PD1 therapy). **b**, Quantification of CD8 IHC in samples with a percentage of PD-L1-positive cells inferior (low PD-L1, $n=40$) or superior (high PD-L1, $n=12$) to 5%. *P* values were calculated using one-sided Wilcoxon test ($P=0.0254$). **c**, Quantification of a PLA showing the ratio of the numbers of pink spots corresponding to the eIF4E–eIF4G interaction per nucleus in samples with low (less than 5%; $n=39$) or high (more than 5%; $n=12$) PD-L1 expression. *P* values were calculated using one-sided Wilcoxon test ($P=0.0017$). **d**, Quantification of PLA showing the ratio of the eIF4E–eIF4G interaction per nucleus in samples from patients who responded (complete response; $n=31$) or did not respond (progressive disease; $n=24$) to anti-PD-1 treatment. *P* values were calculated using one-sided Wilcoxon test ($P=0.0346$). **e**, PLA of PD-1 and PD-L1 are presented for 2 representative tumors from a total of 55 (no. 1 is high and no. 2 is low ratio of PD-1–PD-L1 PLA dots). **f**, Scatter graphs were generated by plotting the PD-1–PD-L1 and eIF4E–eIF4G PLA values for each sample (log). A Spearman test was performed ($n=55$ tumors).

translational effects on IFN-γ-treated cells, we separated mRNAs on the basis of the number of their associated ribosomes by using polysome profiling after short time exposure (2 h) to silvestrol, followed by microarray analysis of polysomal mRNAs. By comparing control cells and IFN-γ-treated cells we observed an upregulation in the level of 685 mRNAs ($\log_2$(fold change) ≤ 1), which corresponds to ~2% of all mRNAs (Fig. 4d, left, and Supplementary Table 1). In the IFN-γ-treated cells, silvestrol led to a decrease in the ribosome recruitment of 569 mRNAs ($\log_2$(fold change) ≤ −1), which corresponds to ~2.8% of all mRNAs analyzed (Fig. 4d, right, and Supplementary Table 2). Then, by crossing mRNAs that are transcriptionally upregulated by IFN-γ and translationally downregulated by silvestrol, we found 23 mRNAs translationally downregulated by silvestrol in IFN-γ-treated cells (Fig. 4e,f). Among these 23 mRNAs (Supplementary Table 3) was the mRNA encoding STAT1, which seemed particularly relevant because of its well-known activity as a transcription factor activated by various ligands, including IFN-γ (ref. [37]). We confirmed that silvestrol inhibited *STAT1* mRNA translation (Fig. 4g,h) without affecting the total level of *STAT1* mRNA (Fig. 4i and Supplementary Fig. 9a). The *STAT1* mRNA harbors a highly structured 5′ untranslated region (5′ UTR) (Supplementary Fig. 9b) with several predicted G quadruplex (G4) RNA secondary structures (Supplementary Fig. 9c), which are potentially regulated by eIF4A[21]. Interestingly, silvestrol as well as PhenDC3, which is a G4 RNA stabilizer[38], inhibited the translation of a chimeric mRNA containing the 5′ UTR of the *STAT1* mRNA inserted upstream of the luciferase open reading frame but did not inhibit the translation of an mRNA containing only the luciferase open reading frame (Fig. 4j and Supplementary Fig. 9d). Consistently, STAT1 protein levels were decreased by silvestrol in a dose-dependent manner (Supplementary Fig. 9e) and increased in $Braf^{V600E}4ebp1^{-/-}4ebp2^{-/-}$ tumors compared with $BRAF^{V600E}$ tumors (Supplementary Fig. 9f). Taken together, these data indicate that eIF4A regulates translation initiation of the *STAT1* mRNA through RNA sequences/secondary structures present in the *STAT1* 5′ UTR.

eIF4F-dependent regulation of STAT1 is a key mediator of inducible PD-L1 expression. To confirm the involvement of STAT1 in PD-L1 expression, we first depleted STAT1 by RNA interference. As expected[37], siRNA-mediated depletion of STAT1 decreased inducible PD-L1 surface expression (Fig. 5a) and *PD-L1* promoter activity (Fig. 5b,c) and therefore phenocopied eIF4F inhibition. Next, to demonstrate that eIF4F-dependent regulation of STAT1 translation controls PD-L1 expression, we ectopically expressed STAT1 from an mRNA devoid of its 5′ UTR. Constitutive expression of STAT1 from the 5′-UTR-less (Δ5′-UTR-*STAT1-GFP*) mRNA was not inhibited by silvestrol and partially overcame eIF4F inhibition of inducible PD-L1 surface expression (Fig. 5d,e). Thus, eIF4F-dependent translational regulation of STAT1 is involved in IFN-γ-induced PD-L1 expression. At later times, eIF4A inhibition led, as expected, to decreased expression of several genes that either constitute direct targets of STAT1 or belong to the IFN-γ signaling pathway (Fig. 5f and Supplementary Fig. 10).

eIF4A inhibition does not impair the functions of activated T cells and has an antitumor effect relying on PD-L1 and the immune system. Given the existence of a coordinated translational–transcriptional axis regulating PD-L1 expression, we explored to what extent eIF4F inhibition could exert an immunotherapeutic effect via PD-L1 downregulation. First, we investigated the consequences of eIF4F inhibition on T cell functions. Silvestrol had no effect on the proliferation of activated T cells (4 days of treatment), the production of cytokines or the cytotoxicity of previously activated T cells (Supplementary Fig. 11a–c). Thus, silvestrol had no significant deleterious effects on the functions of activated T cells, enabling an investigation of the effect of silvestrol on tumor growth

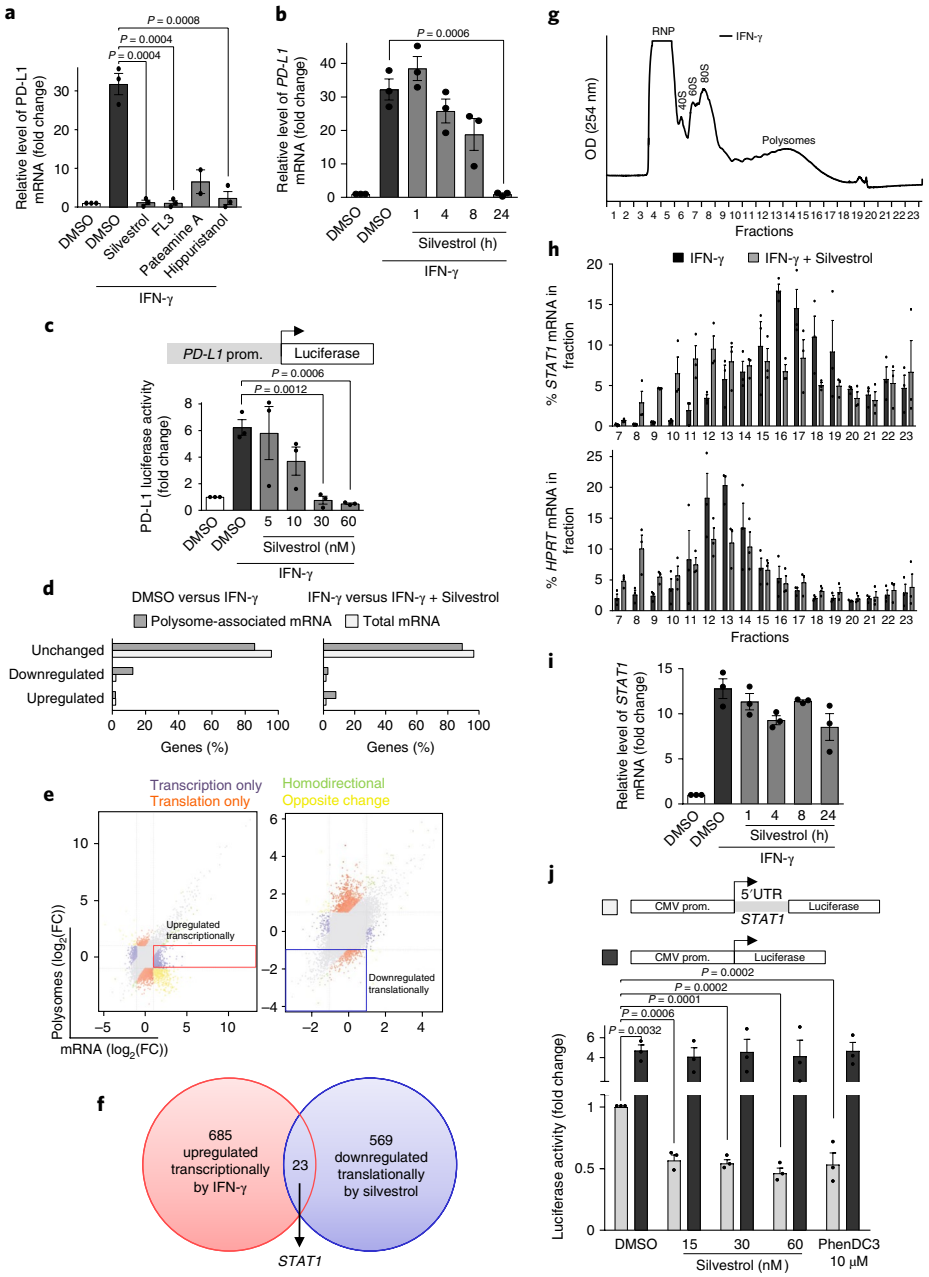

Fig. 4 | eIF4F regulates the translation of the *STAT1* mRNA. a, Relative *PD-L1* mRNA expression in A375 cells treated with silvestrol (30 nM), FL3 (10 nM), pateamine A (10 μM) or hippuristanol (1 μM) in the presence of IFN-γ (200 ng ml^{-1}) for 24 h. Histograms represent the means ± s.e.m. ($n = 3$ independent experiments; but $n = 2$ independent experiments for pateamine A). *P* values were calculated using two-sided unpaired *t*-test. **b**, Relative *PD-L1* mRNA expression in A375 cells treated with IFN-γ (200 ng ml^{-1}) and silvestrol (30 nM). The data are presented as the mean ± s.e.m. ($n = 3$ independent experiments). *P* values were calculated using two-sided unpaired *t*-test. **c**, Analysis of *PD-L1* promoter activity in A375 cells treated with IFN-γ (200 ng ml^{-1}) and silvestrol (30 nM). The results are expressed as the fold change compared with the cells treated with DMSO and are presented as the mean ± s.e.m. ($n = 3$ independent experiments). *P* values were calculated using two-sided unpaired *t*-test. **d**, Frequency of regulated genes among gene probes upregulated ($\log_2$(fold change) > +1), downregulated ($\log_2$(fold change) < −1) or unchanged in A375 cells treated 24 h with IFN-γ (200 ng ml^{-1}) relative to their expression in A375 cells treated with DMSO (left) or A375 cells treated 24 h with IFN-γ and 2 h with silvestrol (30 nM) relative to their expression in A375 cells treated only with IFN-γ (right) in polysome-associated mRNA or total mRNA extracts. **e**, Microarray analysis of RNA isolated from A375 cells treated with IFN-γ relative to their expression in A375 cells treated with DMSO (left) or A375 cells treated with IFN-γ and silvestrol relative to their expression in A375 cells treated only with IFN-γ (right) presented as the correlation of the expression of total mRNA with polysome-associated mRNA. **f**, Overlap (middle) between genes transcriptionally upregulated ($\log_2$(fold change) > +1) in A375 cells treated with IFN-γ relative to A375 cells treated with DMSO (left) and genes translationally downreguled ($\log_2$(fold change) < −1) in A375 cells treated with IFN-γ and silvestrol relative to their expression in A375 cells treated only with IFN-γ (right), as identified in **e**. **g**, Polysome profiles of A375 cells treated 24 h with IFN-γ. One representative profile from three independent expreriments is shown. **h**, Percentage of transcripts in each polysomal fraction obtained by sucrose-gradient ultracentrifugation was quantified by qRT–PCR ($n = 3$). **i**, Relative *STAT1* mRNA expression in A375 cells treated with IFN-γ (200 ng ml^{-1}) and silvestrol (30 nM) ($n = 3$ independent experiments). **j**, Analysis of luciferase activity in A375 cells transfected with the indicated constructs and treated as indicated. The results are expressed as the fold change compared with the cells treated with DMSO. The data are presented as the mean ± s.e.m. ($n = 3$ independent experiments). *P* values were calculated using two-sided unpaired *t*-test.

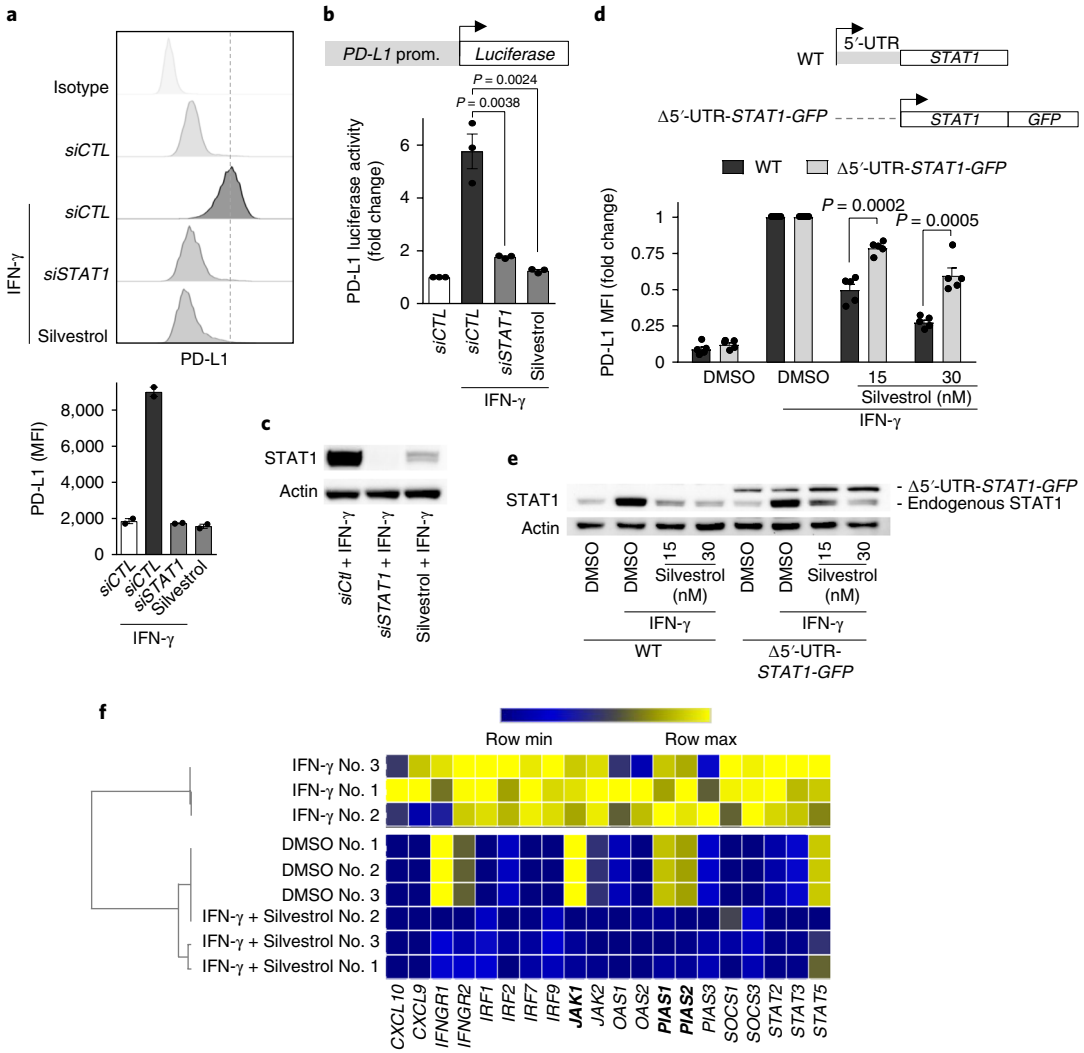

Fig. 5 | eIF4F-dependent regulation of STAT1 is a key mediator of inducible PD-L1. a, PD-L1 is visualized by flow cytometry in A375 melanoma cells transfected with siRNA against STAT1 or siRNA control and treated with IFN-γ and silvestrol. One representative experiment of two is shown (top) and the MFI of PD-L1 is also shown (bottom) ($n = 2$ independent experiments). **b**, Analysis of *PD-L1* promoter activity in A375 melanoma cells transfected with an siRNA against *STAT1* or siRNA control (siCTL) and treated with IFN-γ. Results were expressed as fold change of the basal luciferase activity compared with cells transfected with a siRNA control. Data are means ± s.e.m. ($n = 3$). **c**, A375 cells were lysed and analyzed by western blotting using the indicated antibodies. One representative experiment of three is shown. **d**, PD-L1 visualized by flow cytometry in A375 melanoma wild-type cells or cell with Δ5′ UTR–*STAT1*–*GFP* ectopic expression that were treated with IFN-γ (200 ng ml^{-1}) and the indicated doses of silvestrol. Data are means of ratios compared with IFN-γ treated conditions ($n = 5$ independent experiments). *P* values calculated using two-sided unpaired *t*-test. **e**, A375 cells were lysed and analyzed by western blotting using the indicated antibodies. One representative experiment of three is shown. **f**, Heat map showing the relative mRNA expression measured by qRT–PCR of the indicated genes in A375 melanoma cells treated 24 h with IFN-γ (200 ng ml^{-1}) and silvestrol (30 nM). Genes that do not contain a STAT1 binding site in the promoter and/or enhancer regions (identified with GeneCards) are indicated in bold.

in vivo. To establish an immunocompetent environment, we used a murine *Braf*^{V600E}*Pten*$^{-/-}$ melanoma cell line derived from tumors originating from genetically modified *Tyr:CreERT*$^{2/0}$;*Braf*^{CA};*Pten*$^{lox/lox}$ mice[39].

At a dose of 0.5 mg kg^{-1}, silvestrol exerted a significant antitumor effect on the *Braf*^{V600E}*Pten*$^{-/-}$ tumors grown in C57BL/6 mice (Fig. 6a). As expected on the basis of our previous experiments, silvestrol decreased the expression of STAT1 and PD-L1 in the *Braf*^{V600E}*Pten*$^{-/-}$ tumors grown in the C57BL/6 mice without significant changes in major histocompatibility complex class I expression (Fig. 6b and Supplementary Fig. 12a). Tumors treated with silvestrol also had greater numbers of CD45-positive cells (Fig. 6c), revealing a stronger infiltration of immune cells into the tumors. Strikingly, when tested in nude mice, the same treatment did not have any antitumor effect (Fig. 6d), indicating that the immune system plays a major role in the antitumor response to silvestrol. Immunofluorescence staining, as well as experiments performed in mice depleted from CD8-positve lymphocytes (Fig. 6e–g), revealed that the antitumor activity of silvestrol is mediated by CD8-positive T cells. Thus, in addition to its direct antitumor activity, which can be seen in nude mice using a higher dose (1 mg kg^{-1}) (Supplementary Fig. 12b), silvestrol exerts a significant antitumor activity via the adaptive immune system.

To directly assess the role of PD-L1 in the antitumor effects of silvestrol in C57BL/6 mice, the same experiment was performed using *Braf*^{V600E}*Pten*$^{-/-}$ melanoma cells transfected with a PD-L1-expressing plasmid driven by a cytomegalovirus promoter (Fig. 6h). Convincingly, silvestrol had no antitumor effect on these *Braf*^{V600E}*Pten*$^{-/-}$ tumors constitutively expressing PD-L1 (Fig. 6i) and, as expected, had an antitumor effect comparable with the one

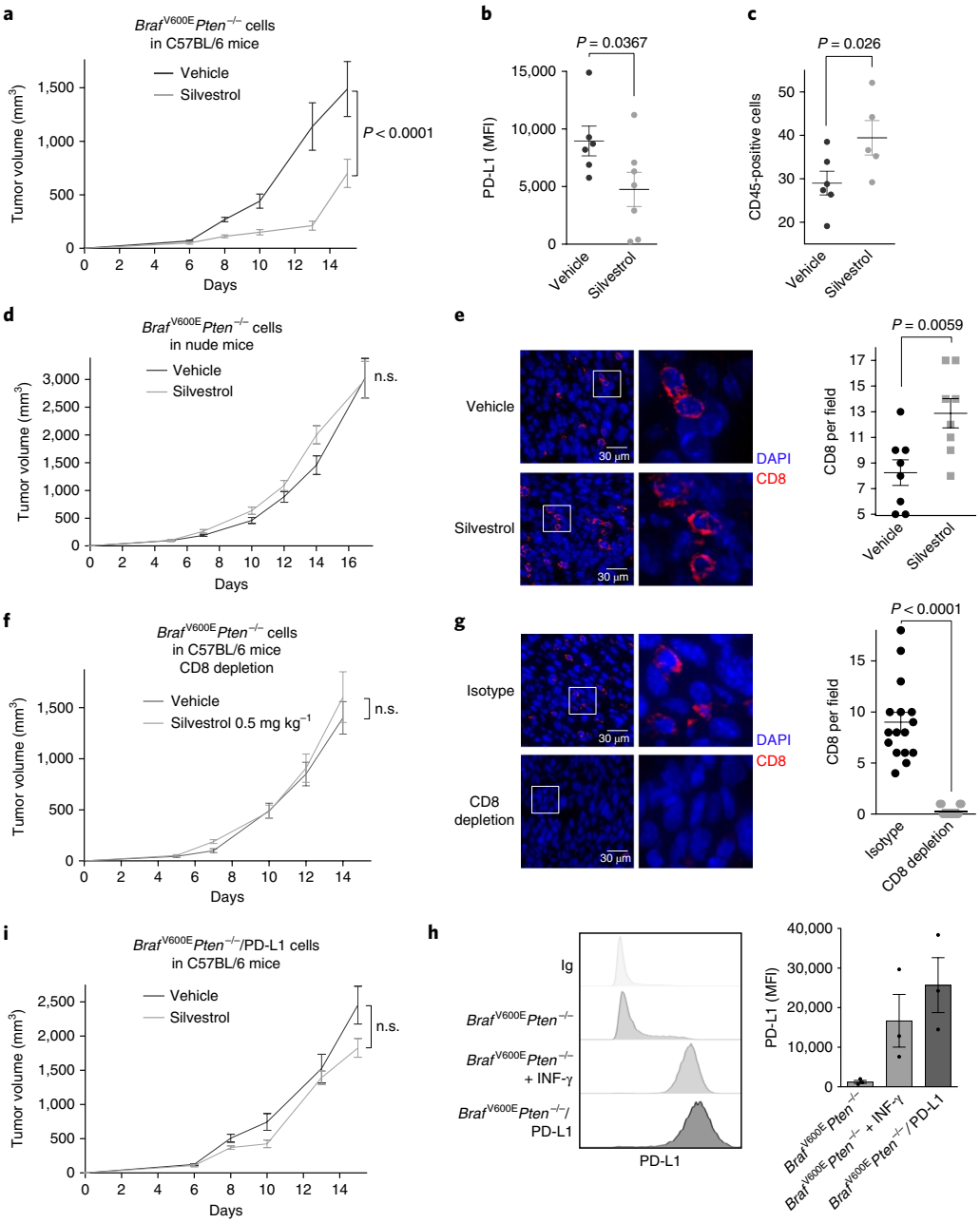

Fig. 6 | Targeting eIF4F inhibits tumor growth via PD-L1 and the immune system. a, C57BL/6 mice were inoculated with murine *Braf*^{V600E}*Pten*$^{-/-}$ (BP) melanoma cells and treated with silvestrol (0.5 mg per kg per day) or vehicle. The data are presented as the mean ± s.e.m. ($n = 8$ mice per group). *P* values were calculated using two-way ANOVA. **b**, PD-L1 expression was determined by flow cytometry in tumors presented in **a**. The data are presented as the mean ± s.e.m. (vehicle $n = 6$ tumors; silvestrol $n = 7$ tumors). *P* values were calculated using one-sided Mann–Whitney test. **c**, Percentage of CD45-positive cells in tumors was determined by flow cytometry in tumors presented in **a**. The data are presented as the mean ± s.e.m. (vehicle $n = 6$ tumors; silvestrol $n = 5$ tumors). *P* values were calculated using one-sided Mann–Whitney test. **d**, Tumor volume in nude mice that were inoculated with BP melanoma cells and treated with silvestrol (0.5 mg per kg per day) or vehicle. The data are presented as the mean ± s.e.m. ($n = 12$ mice per group) *P* values were calculated using two-way ANOVA (n.s., not significant; $P = 0.2618$). **e**, CD8-positive cells were visualized by immunofluorescence on frozen section tumors presented in **a**. DAPI was used to visualize nuclei. Representative tumors are shown on the left and mean ± s.e.m. of CD8-positive cells are shown on the right ($n = 8$ tumors per group). *P* values were calculated using one-sided Mann–Whitney test. **f**, Tumor volume in C57BL/6 mice that were inoculated with BP melanoma cells, treated with an anti-mouse CD8 antibody and silvestrol (0.5 mg per kg per day), or vehicle. The data are presented as the mean ± s.e.m. ($n = 16$ tumors per group). *P* values were calculated using two-way ANOVA (n.s.; $P = 0.5288$). **g**, CD8-positive cells were visualized by immunofluorescence on frozen section tumors presented in **f**. DAPI was used to visualize nuclei. Representative tumors (left) and mean ± s.e.m. of CD8-positive cells (right) are shown (isotype $n = 16$, CD8 depletion $n = 15$ tumors). *P* values were calculated using one-sided Mann–Whitney test. **h**, PD-L1 was visualized by flow cytometry in BP melanoma cells untreated or treated with IFN-γ and BP melanoma cells overexpressing PD-L1. One representative experiment of three is shown (left) and results represent the mean ± s.e.m. (right) ($n = 3$ independent experiments). **i**, Tumor volume in C57BL/6 mice that were inoculated subcutaneously with BP melanoma cells overexpressing PD-L1 and treated with silvestrol (0.5 mg per kg per day) or vehicle. The data are presented as the mean ± s.e.m. ($n = 8$ mice per group). *P* values were calculated using two-way ANOVA (n.s.; $P = 0.0685$).

observed on anti-PD1 antibody treatment (Supplementary Fig. 12c). Therefore, the inhibition of eIF4A in vivo acts as an immune checkpoint immunotherapy with an antitumor effect mediated by the immune system and dependent on PD-L1 downregulation.

Discussion

Our data show that the eIF4F complex controls the expression of PD-L1, a major immune checkpoint. This regulation is indirect since eIF4F regulates the translation of the mRNA encoding STAT1, one of the major *PD-L1* transcriptional regulators, through RNA sequences/secondary structures present in the *STAT1* 5′ UTR. Demonstration of this translation–transcription regulatory cascade is consistent with previous reports suggesting that the initial alteration of the translational efficiency of existing mRNAs encoding transcription factors leads to delayed transcriptional alterations in gene expression profiles as a secondary effect[40]. Importantly, eIF4A inhibition of PD-L1 surface expression is rescued by the ectopic expression of STAT1 from an mRNA devoid of its 5′ UTR, demonstrating the involvement of STAT1 in the eIF4F-dependent regulation of PD-L1. The association between eIF4F complex formation and PD-L1 expression also exists in vivo, first in a genetically modified murine model, where eIF4F complex formation is constitutively upregulated and PD-L1 expression increased, as well as in melanoma samples from patients, where we found a positive correlation between eIF4F complex formation and induced PD-L1 expression.

These findings are significant for several reasons. First, they demonstrate a new and unsuspected link between eIF4F and PD-L1, which are two control checkpoints of paramount importance in cancer biology. On one hand, eIF4F has become an increasingly attractive target for potential anticancer therapeutics[15,16,41]. Indeed, oncogenic signaling is known to stimulate eIF4F complex formation[20,24]. In addition, members of this complex are involved in cell transformation, metastatic processes and chemoresistance[42–45]. Taken together this opens a window on cancer-specific therapeutic opportunities for eIF4F inhibitors. In addition, eIF4F has recently been demonstrated to be directly implicated in targeted anticancer therapy resistance. In particular, we have shown that resistance of BRAF or NRAS mutant cancer cells to BRAF and/or MEK inhibitors is associated with eIF4F activation. In addition, eIF4F inhibitors, used in combination with BRAF inhibitors, are able to rescue tumor cell resistance[20,46]. Several companies are currently developing eIF4F inhibitors, with promising preliminary results[22].

PD-L1 regulation, on the other hand has become an important research topic because of its direct implication in tumor immune escape and in the therapeutic effect of both anti-PD-1 and anti-PD-L1 antibodies[47]. Several mechanisms of PD-L1 expression regulation have recently been published, involving MYC, CSN5, CMTM4 and CMTM6 proteins[8,10–12]. However, these mechanisms are distinct from the one elucidated here because they occur at the transcriptional or post-translational level. Most importantly, they do not concern the regulation of PD-L1 in response to the activated lymphocyte-secreted IFN-γ. It is precisely this inducible PD-L1 expression that is involved when considering the response to anti-PD-1 or anti-PD-L1 antibodies. This is further validated by our findings in melanoma samples from patients, where activation of eIF4F is associated with PD-1–PD-L1 engagement, as well as with response to anti-PD-1 treatment. Two aberrant samples with high PD-L1 expression, low eIF4F activity and low CD8-positive cell counts are good examples of the possible discrepancy between PD-L1 expression and the IFN-γ signaling pathway. This highlights the fact that in some patients, eIF4F could be considered as an additional theranostic marker for PD-1 or PD-L1-based therapies.

Our findings are also noteworthy because of their implications for research in the fields of protein translation and cancer immunotherapy. With regard to protein translation, demonstration of an immune-mediated effect of the eIF4A helicase inhibitor silvestrol was largely unsuspected. This opens new and exciting opportunities for eIF4F inhibitors as immunotherapeutic agents, in addition to their direct antitumor effects. This potential immunotherapeutic action of eIF4F inhibitors is further bolstered by the lack of a deleterious effect of silvestrol on the main immune functions of activated T cells, as we and others have shown[48]. In cancer immunotherapy, although nobody can argue against the potential benefit of a biomarker specifically associated with inducible, as opposed to constitutive, PD-L1 expression, the demonstration of eIF4F as an immunotherapeutic agent seems counterintuitive at first. The main reason for this is that, in patients treated with anti-PD-1, disruption of the IFN-γ pathway has been shown to be associated with resistance to anti-PD-1 agents[49]. In this context, blockade of eIF4F, which downregulates the IFN-γ pathway and consequently leads to decreased PD-L1 expression, may not seem appropriate. However, cancer immune escape results from multiple complex mechanisms[47] and most metastatic patients finally become resistant to anti-PD-1 therapy in spite of a functional IFN-γ pathway. In fact, both IFN-γ and STAT1 have been shown to be capable of exerting both tumor suppressive and tumor promoting functions, depending on the context[50]. The efficacy of IFN-γ in patients with melanoma is mediocre, and prolonged IFN-γ signaling can even induce resistance to checkpoint inhibitors such as anti-CTLA4, as well as anti-PD-1, by upregulating alternative T cell inhibitory receptors[51,52]. This STAT1-dependent chronic resistance highlights the complexity of the T cell inhibitory receptor networks and the need to consider the dynamics of events following immune checkpoint blockade. It has even been proposed that interrupting the IFN-γ pathway using Janus kinase inhibitors could offset the sustained IFN-γ-derived resistance[52]. In this respect, drugs such as eIF4F inhibitors that combine a direct antitumor effect with downregulation of STAT1 and decreased expression of the negative immune checkpoint PD-L1 could be of remarkable therapeutic interest.

Altogether, the relationship that we have identified between the protein translation initiation control and PD-L1 highlights the need for a prompt development of eIF4F inhibitors in patients with cancer, with parallel translational studies of their direct antitumor action as well as their immune-mediated effects.

Online content

Any methods, additional references, Nature Research reporting summaries, source data, statements of data availability and associated accession codes are available at https://doi.org/10.1038/s41591-018-0217-1.

Received: 23 April 2018; Accepted: 24 August 2018;
Published online: 29 October 2018

References

1. Hodi, F. S. et al. Improved survival with ipilimumab in patients with metastatic melanoma. *N. Engl. J. Med.* **363**, 711–723 (2010).
2. Robert, C. et al. Ipilimumab plus dacarbazine for previously untreated metastatic melanoma. *N. Engl. J. Med.* **364**, 2517–2526 (2011).
3. Robert, C. et al. Pembrolizumab versus ipilimumab in advanced melanoma. *N. Engl. J. Med.* **372**, 2521–2532 (2015).
4. Robert, C. et al. Nivolumab in previously untreated melanoma without BRAF mutation. *N. Engl. J. Med.* **372**, 320–330 (2015).
5. Zou, W., Wolchok, J. D. & Chen, L. PD-L1 (B7-H1) and PD-1 pathway blockade for cancer therapy: Mechanisms, response biomarkers, and combinations. *Sci. Transl. Med.* **8**, 328rv4 (2016).
6. Pardoll, D. M. The blockade of immune checkpoints in cancer immunotherapy. *Nat. Rev. Cancer* **12**, 252–264 (2012).
7. Green, M. R. et al. Integrative analysis reveals selective 9p24.1 amplification, increased PD-1 ligand expression, and further induction via JAK2 in nodular sclerosing Hodgkin lymphoma and primary mediastinal large B-cell lymphoma. *Blood* **116**, 3268–3277 (2010).
8. Casey, S. C. et al. MYC regulates the antitumor immune response through CD47 and PD-L1. *Science* **352**, 227–231 (2016).

9. Coelho, M. A. et al. Oncogenic RAS signaling promotes tumor immunoresistance by stabilizing PD-L1 mRNA. *Immunity* **47**, 1083–1099.e6 (2017).
10. Lim, S. O. et al. Deubiquitination and stabilization of PD-L1 by CSN5. *Cancer Cell* **30**, 925–939 (2016).
11. Mezzadra, R. et al. Identification of CMTM6 and CMTM4 as PD-L1 protein regulators. *Nature* **549**, 106–110 (2017).
12. Burr, M. L. et al. CMTM6 maintains the expression of PD-L1 and regulates anti-tumour immunity. *Nature* **549**, 101–105 (2017).
13. Ribas, A. & Hu-Lieskovan, S. What does PD-L1 positive or negative mean? *J. Exp. Med.* **213**, 2835–2840 (2016).
14. Chu, J., Cargnello, M., Topisirovic, I. & Pelletier, J. Translation initiation factors: reprogramming protein synthesis in cancer. *Trends. Cell Biol.* **26**, 918–933 (2016).
15. Truitt, M. L. & Ruggero, D. New frontiers in translational control of the cancer genome. *Nat. Rev. Cancer* **16**, 288–304 (2016).
16. Pelletier, J., Graff, J., Ruggero, D. & Sonenberg, N. Targeting the eIF4F translation initiation complex: a critical nexus for cancer development. *Cancer Res.* **75**, 250–263 (2015).
17. Chu, J., Cajal, S. R. Y., Sonenberg, N. & Pelletier, J. Eukaryotic initiation factor 4F-sidestepping resistance mechanisms arising from expression heterogeneity. *Curr. Opin. Genet. Dev.* **48**, 89–96 (2017).
18. de la Parra, C., Walters, B. A., Geter, P. & Schneider, R. J. Translation initiation factors and their relevance in cancer. *Curr. Opin. Genet. Dev.* **48**, 82–88 (2017).
19. Zindy, P. et al. Formation of the eIF4F translation-initiation complex determines sensitivity to anticancer drugs targeting the EGFR and HER2 receptors. *Cancer Res.* **71**, 4068–4073 (2011).
20. Boussemart, L. et al. eIF4F is a nexus of resistance to anti-BRAF and anti-MEK cancer therapies. *Nature* **513**, 105–109 (2014).
21. Wolfe, A. L. et al. RNA G-quadruplexes cause eIF4A-dependent oncogene translation in cancer. *Nature* **513**, 65–70 (2014).
22. Bhat, M. et al. Targeting the translation machinery in cancer. *Nat. Rev. Drug Discov.* **14**, 261–278 (2015).
23. Steinberger, J., Chu, J., Maiga, R. I., Sleiman, K. & Pelletier, J. Developing anti-neoplastic biotherapeutics against eIF4F. *Cell. Mol. Life Sci.* **74**, 1681–1692 (2017).
24. Malka-Mahieu, H., Newman, M., Desaubry, L., Robert, C. & Vagner, S. Molecular pathways: the eIF4F translation initiation complex-new opportunities for cancer treatment. *Clin. Cancer Res.* **23**, 21–25 (2017).
25. Barretina, J. et al. The cancer cell line encyclopedia enables predictive modelling of anticancer drug sensitivity. *Nature* **483**, 603–607 (2012).
26. Sadlish, H. et al. Evidence for a functionally relevant rocaglamide binding site on the eIF4A-RNA complex. *ACS Chem. Biol.* **8**, 1519–1527 (2013).
27. Chu, J. et al. CRISPR-mediated drug-target validation reveals selective pharmacological inhibition of the RNA Helicase, eIF4A. *Cell Rep.* **15**, 2340–2347 (2016).
28. Bordeleau, M. E. et al. Therapeutic suppression of translation initiation modulates chemosensitivity in a mouse lymphoma model. *J. Clin. Invest.* **118**, 2651–2660 (2008).
29. Cencic, R. et al. Antitumor activity and mechanism of action of the cyclopenta[*b*]benzofuran, silvestrol. *PLoS ONE* **4**, e5223 (2009).
30. Rubio, C. A. et al. Transcriptome-wide characterization of the eIF4A signature highlights plasticity in translation regulation. *Genome Biol.* **15**, 476 (2014).
31. Bordeleau, M. E. et al. Functional characterization of IRESes by an inhibitor of the RNA helicase eIF4A. *Nat. Chem. Biol.* **2**, 213–220 (2006).
32. Bordeleau, M. E. et al. Stimulation of mammalian translation initiation factor eIF4A activity by a small molecule inhibitor of eukaryotic translation. *Proc. Natl Acad. Sci. USA* **102**, 10460–10465 (2005).
33. Dhomen, N. et al. Oncogenic Braf induces melanocyte senescence and melanoma in mice. *Cancer Cell* **15**, 294–303 (2009).
34. Le Bacquer, O. et al. Elevated sensitivity to diet-induced obesity and insulin resistance in mice lacking 4E-BP1 and 4E-BP2. *J. Clin. Invest.* **117**, 387–396 (2007).
35. Colina, R. et al. Translational control of the innate immune response through IRF-7. *Nature* **452**, 323–328 (2008).
36. Lin, C. J. et al. Targeting synthetic lethal interactions between Myc and the eIF4F complex impedes tumorigenesis. *Cell Rep.* **1**, 325–333 (2012).
37. Garcia-Diaz, A. et al. Interferon receptor signaling pathways regulating PD-L1 and PD-L2 expression. *Cell Rep.* **19**, 1189–1201 (2017).
38. Halder, K., Largy, E., Benzler, M., Teulade-Fichou, M. P. & Hartig, J. S. Efficient suppression of gene expression by targeting 5′-UTR-based RNA quadruplexes with bisquinolinium compounds. *Chembiochem* **12**, 1663–1668 (2011).
39. Cooper, Z. A. et al. Response to BRAF inhibition in melanoma is enhanced when combined with immune checkpoint blockade. *Cancer Immunol. Res.* **2**, 643–654 (2014).
40. Rajasekhar, V. K. et al. Oncogenic Ras and Akt signaling contribute to glioblastoma formation by differential recruitment of existing mRNAs to polysomes. *Mol. Cell* **12**, 889–901 (2003).
41. Chu, J. & Pelletier, J. Targeting the eIF4A RNA helicase as an anti-neoplastic approach. *Biochim. Biophys. Acta* **1849**, 781–791 (2015).
42. Lazaris-Karatzas, A., Montine, K. S. & Sonenberg, N. Malignant transformation by a eukaryotic initiation factor subunit that binds to mRNA 5′ cap. *Nature* **345**, 544–547 (1990).
43. Graff, J. R. et al. Reduction of translation initiation factor 4E decreases the malignancy of ras-transformed cloned rat embryo fibroblasts. *Int. J. Cancer* **60**, 255–263 (1995).
44. Wendel, H. G. et al. Survival signalling by Akt and eIF4E in oncogenesis and cancer therapy. *Nature* **428**, 332–337 (2004).
45. Wendel, H. G. et al. Determinants of sensitivity and resistance to rapamycin-chemotherapy drug combinations in vivo. *Cancer Res.* **66**, 7639–7646 (2006).
46. Malka-Mahieu, H. et al. Synergistic effects of eIF4A and MEK inhibitors on proliferation of NRAS-mutant melanoma cell lines. *Cell Cycle* **15**, 2405–2409 (2016).
47. Sharpe, A. H. & Pauken, K. E. The diverse functions of the PD1 inhibitory pathway. *Nat. Rev. Immunol.* **18**, 153–167 (2018).
48. Patton, J. T. et al. The translation inhibitor silvestrol exhibits direct anti-tumor activity while preserving innate and adaptive immunity against EBV-driven lymphoproliferative disease. *Oncotarget* **6**, 2693–2708 (2015).
49. Zaretsky, J. M. et al. Mutations associated with acquired resistance to PD-1 blockade in melanoma. *N. Engl. J. Med.* **375**, 819–829 (2016).
50. Meissl, K., Macho-Maschler, S., Muller, M. & Strobl, B. The good and the bad faces of STAT1 in solid tumours. *Cytokine* **89**, 12–20 (2017).
51. Benci, J. L. et al. Tumor interferon signaling regulates a multigenic resistance program to immune checkpoint blockade. *Cell* **167**, 1540–1554.e12 (2016).
52. Reading, J. L. & Quezada, S. A. Too much of a good thing? Chronic IFN fuels resistance to cancer immunotherapy. *Immunity* **45**, 1181–1183 (2016).

Acknowledgements

We thank M. A. Shipp for the PD-L1 luciferase promoter, J. Wargo for the BRAF/PTEN mouse cell line (BP), S. Rocchi for the CMVβGal plasmid and WM793 melanoma cells and M.-P. Teulade-Fichou for the PhenDC3. We thank the Institut Curie Genomics (A. Rapinat and D. Gentien) platform for assistance with the microarray experiments and the animal facility of the Orsay site of the Institut Curie. We thank the Gustave Roussy platform 'Module de developpement en pathologie INSERM U981/SIRI SOCRATE' and 'Plateforme d'évaluation Préclinique'. We thank M. Tichet, M. Khaled and S. Apcher for helpful discussions. This study was supported by INSERM, CNRS, Gustave Roussy and Institut Curie. This study was also funded by grants from Ligue Nationale Contre le Cancer (Equipe labellisée) (to S.V. and A.E.), Institut National du Cancer (grant number 2013-1-MEL-01-ICR-1) (to S.V., A.E. and C.R.), 'Ensemble contre le mélanome' (to C.R. and S.V.), 'Vaincre le Mélanome' (to M.C. and C.R.), Les Sites de recherche Intégré sur le Cancer (SIRIC Socrate) label Gustave Roussy (to C.R.), Fondation Bettencourt Schueller (to C.R.) and Fondation ARC pour la Recherche sur le Cancer (project PJA20161204588) (to S.S.). M.C. was supported by a post-doctoral fellowship from 'Association pour la recherche contre le cancer' and R.G. was supported by a pre-doctoral fellowship from 'Fondation pour la Recherche Médicale, (FDT2017043739).

Author contributions

M.C. and R.G. designed and performed in vitro and in vivo experiments and analyzed data. H.M.-M. established the silvestrol-resistant cell line, the *Braf*^{V600E}*4ebp1*$^{-/-}$*4ebp2*$^{-/-}$ cell lines and performed associated experiments. S.D., C.E. and A.E. established the *Braf*^{V600E}*4ebp1*$^{-/-}$*4ebp2*$^{-/-}$ mouse model and *Braf*^{V600E}*4ebp1*$^{-/-}$*4ebp2*$^{-/-}$ cell lines and analyzed data. S.S. contributed to microarray data analysis. D.A. contributed to in vivo experiments. I.G., C.W. and S.A. performed experiments on patient samples and analyzed data. S.M. performed polysomal fractionation. J.A. and J.Y.S. analyzed IHC and PLA on human samples. C.L., E.R. and S.R. provided clinical samples. L.D. provided FL3. N.S., A.M.E. and A.E. gave advice; M.C., S.V. and C.R. wrote the manuscript. M.C. and R.G. share first authorship; S.D., I.G. and H.M.-M. share second authorship; S.V. and C.R. supervised all research and are joint senior authors.

Competing interests

C.R. is an occasional consultant to Merck Sharp and Dohme, Bristol-Myers Squibb, Merck and Roche. All other authors have no competing interests.

Additional information

Supplementary information is available for this paper at https://doi.org/10.1038/s41591-018-0217-1.

Reprints and permissions information is available at www.nature.com/reprints.

Correspondence and requests for materials should be addressed to S.V. or C.R.

Publisher's note: Springer Nature remains neutral with regard to jurisdictional claims in published maps and institutional affiliations.

Methods

Cell lines and reagents. The A375, A2058, SKMel28, SKMel2 (human melanoma) and 4T1 (murine mammary carcinoma) cell lines used in this study were purchased from the American Type Culture Collection. The human melanoma SKMel10 cell line was a gift from L. Zitvogel. The melanoma BP cell line was a gift from J. Wargo. The human melanoma WM793 cell line was a gift from S. Rocchi. The human colon adenocarcinoma HT29 cell line was a gift from C. Nahmias. The human lung carcinoma A549 cell line was a gift from J. C. Soria. The human breast adenocarcinoma MCF7 cell line was a gift from F. André. Cancer cell lines were maintained at 37 °C and 5% CO_2 in a humidified atmosphere and grown in RPMI 1640, DMEM or Ham's F-12 growth medium supplemented with 10% FBS, 50 µg ml^{-1} penicillin and 50 mg ml^{-1} streptomycin (Gibco). All cell lines were regularly verified to be mycoplasma free using a PCR-based test (Biovalley). The cells were treated with IFN-γ (PeproTech) dissolved in PBS, and the eIF4A inhibitors (that is, silvestrol, FL3, pateamine A and hippuristanol) were dissolved in DMSO prior to in vitro studies. Silvestrol was purchased from MedChem Tronica, FL3 was provided by L. Désaubry, pateamine A was provided by S. Apcher, hippuristanol was provided by J. Tanaka and the G4 RNA stabilizer was a gift from M.-P. Teulade-Fichou.

Flow cytometry analysis. Cells were detached using Versene (Thermo Scientific), resuspended in PBS/EDTA/BSA containing Fc Block (BD Biosciences), centrifuged, incubated for 30 min with primary antibodies, washed with PBS/EDTA/BSA containing 7AAD or Zombie NIR and then resuspended in 300 µl PBS/EDTA/BSA. The stained cells were analyzed using a LSRII flow cytometer (BD Biosciences). Data were analyzed using FlowJo software. Data were collected, debris (low FSC and SCC) was excluded and single cells that were negative for the live/dead discriminant were gated.

The following specific antibodies were purchased from BioLegend and used for the flow cytometry analysis: human PD-L1 (329708), mouse PD-L1 (124312) and mouse CD45 (103128). An isotype was used as a nonspecific control according to the datasheet supplied with each antibody.

Mice tumor dissociation. Tumors from the mice were digested for 1–2 h with collagenase A (0.33 U ml^{-1}), Dispase (0.85 U ml^{-1}) and DNase I (144 U ml^{-1}) under rapid shaking at 37 °C. Large debris was removed by filtration through a 70-µm cell strainer, and the cells were then stained using the cell line procedure.

siRNA transfection. Transfection of duplex siRNAs (50 nmol l^{-1}) was performed using Lipofectamine RNAiMAX (Invitrogen) in Opti-MEM (Invitrogen) as previously described[53]. The day after transfection, IFN-γ (200 ng ml^{-1}) was added to the medium and the proteins extracted after 24 h. The sequences and/or catalog numbers of the specific siRNAs are available on request. A siRNA targeting luciferase was used as a nonspecific control[54].

Western blot assays. Immunoblotting was performed using whole-cell lysates prepared in buffer containing 50 mM, TRIS-HCl, pH 7.5, 15 mM NaCl, 1% Triton X-100 and 1× protease and phosphatase inhibitor (Roche). The protein content in the cell lysates was quantified using a bicinchoninic acid protein assay kit (Thermo). Protein samples were resolved on NuPAGE gels (Life Technologies) and transferred to a 0.45-mm nitrocellulose membrane (Bio-Rad). After saturation in a buffer containing TRIS-HCl, NaCl, EDTA and Tween-20, the gelatin and BSA membranes were incubated with the appropriate antibodies. Proteins were visualized using an ECL system (Bio-Rad).

Antibodies specific for the following proteins were purchased from Cell Signaling Technologies: eIF4G (2498), 4E-BP1 (9644), 4E-BP2 (2845), eIF4E (2067), eIF4A1 (2490) and STAT1 (9172). Antibody specific for GAPDH (MAB374) was purchased from Millipore. The antibody specific for β-actin (A5060) was purchased from Sigma. The antibody specific for HSP90 was purchased from Santa Cruz Biotechnology (13119). Horseradish peroxidase (HRP)-conjugated secondary antibodies were purchased from Sigma.

Proliferation assay. Cell proliferation was measured using WST-1 reagent (Roche Applied Science). Melanoma cells (5,000) were plated in 96-well tissue culture plates. After 24 h, cells were treated with drugs or DMSO at the indicated concentrations, in triplicate. WST-1 reagent was added to the wells and incubated at 37 °C for 2 h before and after the treatment period of 48 h. The plates were then read at 450 nm on a Victor Multilabel Counter model 1420 (Perkin Elmer). Cell proliferation is expressed as a percentage of the absorbance compared with mock-treated cells.

pR–HepC–L bicistronic dual luciferase reporter assays. In this assay, translation of the first (LucR) cistron is eIF4F dependent, while translation of the hepatitis C virus internal ribosome entry site-driven second (LucF) cistron is eIF4F independent. Differential translation of both cistrons, as measured by the ratio of luciferase activities, directly reflects differences in eIF4F activity. Dual luciferase assays were conducted in A375 and A375-SR cells transfected with 50 ng of pR–HepC–L bicistronic vector in 96-well plates using Lipofectamine 2000 reagent (Life Technologies). The lysates were prepared in triplicate with the Dual-Luciferase Reporter Assay System (Promega), and 10 µl firefly and Renilla bioluminescence lysates were measured with the Centro LB960 Microplate Luminometer (Berthold Technologies) ($n = 3$).

Microfluidic western blotting. Microfluidic western blotting was performed using the Simple WesternWes system (ProteinSimple), a combination of capillary electrophoresis and immunodetection techniques, following the manufacturer's protocols.

Briefly, 1 µg of whole-cell lysate (final concentration of 0.2 µg µl^{-1}) was mixed with 5× fluorescent master mix containing SDS, DTT (40 mM) and fluorescent molecular weight standards, and heated at 95 °C for 5 min. Samples, plus biotinylated molecular weight standards, were loaded along with blocking reagent, primary antibodies against STAT1 (1:500, Cell Signaling), CMH-I H2kb (1:50, Thermofisher), β–actin–HRP (1:1,000, Novus Biologicals), Vinculin (1:50, Santa Cruz), MYC (1:25, Santa Cruz), IFR7 (1:50, Abcam), HRP-conjugated secondary antibodies, wash buffer and chemiluminescent substrate into a microplate prefilled with staking and separation matrices. Fully automated western blotting was performed: proteins were separated by electrophoresis at 375 V for 25 min, immobilized to the capillary by UV crosslinking and incubated with primary and secondary antibodies for 30 min each. Chemiluminescent signal was captured by a CCD (charge-coupled device) camera and the resulting image was anayzed by Compass software (ProteinSimple) and expressed as peak intensity. Quantification was performed by normalizing areas under protein peaks to β-actin and Vinculin loading controls.

Generation of the *4ebp1*$^{-/-}$;*4ebp2*$^{-/-}$;*Braf*$^{+/LSL\text{-}V600E}$;*Tyr::CreERT2/*$^{+}$ mouse model. The *4ebp*$^{-/-}$(ref. [55]), *4ebp2*$^{-/-}$(ref. [56]), *Braf*$^{+/LSL\text{-}V600E}$(ref. [33]) and *Tyr::CreERT2/*$^{+}$ (ref. [57]) mice have been previously described. The strains were interbred on a pure C57BL6 genetic background, and genotyping was performed as previously reported[33,55–57]. The *4ebp1*$^{+/+}$;*4ebp2*$^{+/+}$;*Braf*$^{+/LSL\text{-}V600E}$;*Tyr::CreERT2/*$^{+}$ animals served as controls, and the *4ebp1*$^{-/-}$;*4ebp2*$^{-/-}$;*Braf*$^{+/LSL\text{-}V600E}$;*Tyr::CreERT2/*$^{+}$ mice served as the knockout animals. To induce BRAF-V600E expression specifically in melanocytes, four doses of tamoxifen (10 mg) were applied to the shaven backs of approximately 2-month-old mice over 7 days. The mice were macroscopically analyzed weekly after shaving to observe occurrence of tumors and signs of morbidity. The establishment of the melanoma cell lines from the primary tumors and tumor transplantations were performed as previously described[58]. Experimental procedures were performed according to the recommendations of the European Union (86/609/EEC) and French National Committee (87/848). Animal care and use were approved by the ethics committee of the Curie Institute in compliance with institutional guidelines.

Proximity ligation assay. The proximity ligation assay is a sensitive technique for studying protein–protein interactions in cells. Two primary antibodies, raised in distinct species, are used to recognize two proteins of interest (here PD-1 and PD-L1 or eIF4E and eIF4G).

Next, a pair of secondary antibodies (PLA probes) that are conjugated to complementary oligonucleotides and directed against the constant regions of each primary antibody (PLUS probe and MINUS probe) are used. When the two target proteins are in close proximity (nominally within 40 nm), and the appropriate substrates and enzymes are added, the MINUS and PLUS probes can participate in a rolling-circle DNA synthesis.

Subsequent addition of a polymerase and HRP-labeled oligonucleotides results in an amplified rolling circular product. The signal resulting from each ligated pair of PLA probes is then visualized as an individual spot. These PLA signals can be quantified (counted) and assigned to a specific subcellular location based on microscopic images

PLAs were performed on both fixed and permeabilized murine melanoma cell lines and on 3-µm human melanoma tissue sections. Following dewaxing and rehydrating of the tissue sections, antigen retrieval was performed by heating the slides at 95 °C for 30 min in Tris/EDTA buffer, pH 9, for interactions between eIF4E and eIF4G, or for 45 minutes in citrate buffer, pH 6, for interactions between PD-1 and PD-L1. Then, the tissue sections and the fixed permeabilized cells were treated identically and the PLA protocol was followed according to the manufacturer's instructions (Olink Bioscience) and included an overnight incubation with the primary antibodies at 4 °C. After blocking, the antibodies were used at the following concentrations: eIF4E (mouse, clone A-10, 1:200; Santa Cruz Biotechnology, 271480,) and eIF4G (rabbit, 1:200; Cell Signaling Technology, 2498) or anti-PD-L1 (rabbit, clone SP142, 1:50 dilution; Spring Bioscience) and anti-PD-1 (mouse, clone NAT105, 1:200 dilution; Abcam). The PLA MINUS and PLA PLUS probes (containing secondary antibodies conjugated to oligonucleotides) were added and incubated for 1 h at 37 °C. More oligonucleotides were then added and allowed to hybridize to the PLA probes. Ligase was used to anneal the two hybridized oligonucleotides into a closed circle. The DNA was then amplified (with rolling-circle amplification) and the amplicons were detected using the Brightfield detection kit for chromogenic development or Far Red detection kit for fluorescence. For PLAs performed on cell lines, nuclei were stained with Olink mounting medium containing DAPI. The results were obtained with a scanner (Olympus VS120) and the number of PLA signals per cell were counted

(>3 fields) by semiautomated image analysis software (ImageJ and CellProfiler). For eIF4E–eIF4G PLAs on tissue sections, purple counterstaining with 3,3′,5,5′-tetramethylbenzidine chromogen for the amplification step was performed. Slides were digitized using a VS120 virtual slide microscope (Olympus) at ×20 magnification and visualized with OlyVIA software in the tumor area.

For PD-1–PD-L1 PLAs on tissue sections, purple counterstaining with haematoxylin chromogen was performed. Regions of interest for image analysis were selected in tumor areas containing both tumor cells and tumor-infiltrating lymphocytes. Cropped RGB images were opened in MacBiophotonics ImageJ software. A composite image was created with the XsRGB macro to increase the signal of dots. This composite image was split into red, green and blue channels. The green channel was used to detect and count the number of nuclei and the red channel to detect and quantify the number of dots. The results were reported as the ratio of the number of dots to the number of detected cell nuclei.

Preparation of lymphocyte-conditioned medium. A medium unconditioned or conditioned by activated lymphocytes was collected, centrifuged at 2,500*g* for 5 min and filtered through 0.22-µm filters to eliminate cell debris. The medium was then supplemented with A375 melanoma cells for 24 h with/without IFN-γ and silvestrol.

Clinical samples. Patients with metastatic melanoma were treated with an anti-PD-1 antibody (nivolumab or pembrolizumab). Patients received appropriate information and signed an informed consent form authorizing tumor biopsies and molecular studies in the context of an institutional CRB-approved protocol (MSN-08-027). Tumors were biopsied before treatment.

Immunohistochemistry of human samples. PD-L1 immunohistochemistry was performed using a Ventana Benchmark Ultra platform following a protocol designed to detect PD-L1 expression in both tumor and immune cells with high sensitivity. Sections (3-µm thick) were deparaffinized and antigen retrieval was performed for 64 min in cell conditioning 1 (CC1) Tris-based buffer. The anti-PD-L1 antibody (clone E1L3N, Cell Signaling Technology) was incubated at 1 µg ml^{-1} for 32 min at room temperature. An anti-rabbit HRP-coupled OptiView detection kit was used according to the manufacturer's recommendations. 3,3'-Diaminobenzidine was used as a chromogen. Each run included tonsil tissue as an external positive control. The percentage of tumor cells with linear membranous PD-L1 staining (continuous or not) at any intensity, and the percentage of the stromal area, including the invasive margin, covered by immune cells stained positive for PD-L1 were scored by a pathologist who was trained to evaluate PD-L1 and who was blinded to the clinical data. No significant melanin deposition in the tumor was observed to interfere with the pathological assessment of the IHC analysis in this case series.

CD8 immunohistochemistry was performed using a Ventana Discovery Ultra platform. After deparaffinization, epitope retrieval was performed for 32 min in CC1 buffer. The primary anti-CD8 antibody (clone SP16, Spring Bioscience) was incubated for 1 h at 37 °C. An antirabbit Ultra-MAP kit coupled to HRP was used for detection. A purple chromogen was used for detection. The CD8 infiltrate was scored by two independent pathologists at both the invasive margin of the tumor and in the tumor using a four-grade scale depending on the density. A consensus was reached in cases of disagreement.

mRNA preparation and real-time/quantitative PCR. mRNA isolation was performed using TRIzol (Invitrogen) according to standard procedures. qRT–PCR was performed using a Luminaris Color Probe qPCR Master Mix (Thermo Scientific) and SuperScript IV Reverse Transcriptase (Thermo Scientific) and was monitored on a Viia 7 System (Applied Biosystems). The *TBP* or *HPRT* gene was used to normalize the results. The primer sequences of each cDNA were designed using Primer-BLAST and are available on request.

For the heat map derived from qRT–PCR data (Fig. 5f), we used the relative quantity values in the MORPHEUS software from The Broad Institute (https://software.broadinstitute.org/morpheus/).

PD-L1 promoter luciferase assays. Melanoma cells were seeded in a 24-well plate and transient transfections were conducted the following day using 2 µl Lipofectamine (Gibco-BRL) and 0.3 µg of pGL3-PD-L1p[7] in a 200-µl final volume. Next, 0.01 µg of pRL Renilla Luciferase Control Reporter Vector (Promega) was cotransfected to control the variability of the transfection efficiency in the reporter assays. One day after the transfection, IFN-γ and silvestrol were added to the medium, or the cells were retransfected with an siRNA against STAT1 or an siRNA control. Then, 24 h after the stimulation or 48 h after the siRNA transfection, the lysates were prepared in triplicate using the Dual-Luciferase Reporter Assay System (Promega) according to the datasheet. The firefly and *Renilla* bioluminescence lysates were measured using a Centro XS^3 LB 960 Microplate Luminometer (Berthold Technologies).

Polysomal fractionation and microarray experiment. Sucrose density gradient centrifugation was performed to separate the subpolysomal and polysomal ribosome fractions. Fifteen minutes prior to collection, the cells were incubated at 37 °C with 100 mg ml^{-1} cycloheximide. Next, the cells were washed, scraped into ice-cold PBS supplemented with 100 mg ml^{-1} cycloheximide, centrifuged at 3,000 r.p.m. for 5 min and then collected into 400 ml of LSB buffer (20 mM Tris, pH 7.4, 100 mM NaCl, 3 mM $MgCl_2$, 0.5 M sucrose, 2.4% Triton X-100, 1 mM DTT, 100 U ml^{-1} RNasin and 100 µg ml^{-1} cycloheximide). After homogenization, 400 ml LSB buffer supplemented with 0.2% Triton X-100 and 0.25 M sucrose were added. The samples were centrifuged at 12,000*g* for 10 min at 4 °C. The resulting supernatant was adjusted with 5 M NaCl and 1 M $MgCl_2$. The lysates were loaded onto a 15–50% sucrose density gradient and centrifuged in an SW41 rotor at 38,000 r.p.m. for 2 h at 4 °C. The polysomal fractions were monitored and collected using a gradient fractionation system (Isco). Total RNA was extracted from the nine heaviest fractions and input samples using the TRIzol method. The microarray experiments were performed in triplicate using Human Clariom d (Affymetrix). For the qRT–PCR experiments, total RNA was extracted using the TRIzol method from 300 ml of each fraction. cDNA was prepared using SuperScript IV Reverse Transcriptase (Thermo Scientific) with random hexamer primers according to the manufacturer's instructions. The same volume of cDNA from each fraction was used to perform the qPCR experiments.

Translation efficiency analysis. Exon array raw data CEL files were processed using Affymetrix expression console software. The data were then normalized using the SST-RMA method with the default settings. Gene expression counts based on the exon alignments were used to statistically model the polysome profiling data using R software. The translation efficiency was calculated using Xtail software. Briefly, for each gene, the normalized read counts of total mRNAs or polysome-bound mRNAs in all samples were used to fit the negative binomial (NB) distribution with dispersions, α, and means, μ. The mRNA count K for gene j in sample i was described as $K_{ji} \sim \mathrm{NB}(\mu_{ji},\alpha_{ji})$. The raw gene expression data were then scaled by a normalization factor based on the median-of-ratios normalization method using DESeq2, and the posterior mean and dispersion of both the total mRNA and polysome mRNA were estimated separately for each gene using empirical Bayes shrinkage. Xtail was then used to define the translational variation across two conditions as the difference between the $\log_2$(fold change) ($\log_2$(FC)) of the polysome mRNA and total mRNA. This procedure established a probability distribution for the translational changes, which was used to infer the statistical significance of the differential translations. The posterior probability of a given coefficient β_j was calculated as $\log Pr(\beta_j) = \Sigma \log f_{\mathrm{NB}}(K_{ji},\mu_{ji}(\beta_{ji}),\alpha_{ji})$. Finally, Xtail tests were performed for each gene regardless of whether a significant difference was observed between the $\log_2$(FC) of the polysome mRNA and that of the total mRNA between the two conditions. Genes with a $\log_2$(FC) greater than 1 ($P < 0.05$) were considered significant genes, allowing us to identify the groups of genes regulated only at the translational or transcriptional level. Genes that were upregulated at the transcriptional level under IFN-γ conditions and downregulated at the translational level under IFN-γ + silvestrol conditions were further studied in subsequent experiments.

STAT1 5′ UTR luciferase assays. Melanoma cells were seeded in a 24-well plate, and transient transfections were conducted the following day using 2 µl Lipofectamine (Gibco-BRL) and 0.3 µg of vector containing the 5′ UTR of STAT1 and the *Renilla* Luciferase or only the *Renilla* Luciferase synthesized by Integrated DNA Technologies in a 200-µl final volume. Next, 0.01 µg of pCMVβGal[53] was cotransfected to control the variability of the transfection efficiency in the reporter assays. One day after the transfection, silvestrol or PhenDC3 was added to the medium. After 24 h, the lysates were prepared in triplicate in the passive lysis buffer (Promega) according to the datasheet. Bioluminescence was measured using a Centro XS^3 LB 960 Microplate Luminometer (Berthold Technologies) and the *Renilla* Luciferase Reporter Assay System (Promega) according to the datasheet, and β-galactosidase activity was assessed by measuring the absorbance at 420 nm after 30 min of incubation with *ortho*-nitrophenyl-β-galactoside at 37 °C.

T cell isolation. Human T cells or specific CD8-positive T cells were enriched from healthy donor blood using RosetteSep Human T Cells or CD8-positive T Cells Enrichment Cocktail with SepMate-50 tubes (StemCell; 15061, 15063, 85450). The purity was determined to be >90% by flow cytometry. The cells were frozen in FBS 10% DMSO until use.

T cell culture. Thawed T cells were cultured in ImmunoCult-XF T Cell Expansion Medium (StemCelll; 10981) and stimulated with ImmunoCult Human CD3/CD28 T Cell Activator Cocktail (StemCell; 10991) in the presence of 100 UI ml^{-1} recombinant human interleukin-2 (IL-2; StemCell, 78036).

T cell proliferation assay. Thawed T cells were stained with 5 µM of carboxyfluorescein diacetate succinimidyl ester obtained from the Cell Division Tracker Kit (BioLegend, 423801) and then stimulated with CD3/CD28 T Cell Activator Cocktail. DMSO or the indicated concentration of silvestrol (HY-13251) was added on day 3 to assess the effects on the proliferation of activated T cells.

On day 7, proliferation was visualized by flow cytometry as a decrease in fluorescence intensity compared with the control, and the proliferation percentage was calculated relative to the DMSO control.

T cell cytokine production. Thawed T cells were cultured and stimulated as mentioned above for 3 d. On day 3, Brefeldin A and Monensin were added to phorbol 12-myristate 13-acetate ionomycin in the presence of DMSO or silvestrol at the indicated concentrations. After 6 h, the cells were stained with Zombie NIR (fixable live/dead discriminant; BioLegend, 423106) and then intracellularly stained with fluorescent anti-TNF-α, anti-IFN-γ or anti-IL-2 (BioLegend). The results were visualized by flow cytometry. Relative cytokine production was calculated compared with the DMSO control.

Cytotoxicity assay. Thawed T cells were cultured and stimulated as described above for 4–5 d. The A375 cells were stained with 5 µM of the Vybrant CFDA SE Cell Tracer Kit (Thermo Fisher, V12883) and plated in a 96-well plate overnight to adhere on day 0. On the following day, T cells were added at different ratios in the presence of silvestrol (30 nM) or DMSO and cocultured with the tumor cells. After 6 h, the adherent cells were washed twice with PBS and fixed with 4% paraformaldehyde, and then the fluorescence intensity remaining in the well was measured using a Victor X4 Plate Reader (PerkinElmer). The percentage of specific lysis was calculated as the decrease in fluorescence in the wells compared with the control well without the T cell addition. The fluorescence intensity in the wells was proportional to the cell number in each well (data not shown). Thus, the remaining fluorescence was representative of the remaining live adherent cells in each well at the end of the experiment.

Mouse graft study. The animals were housed under pathogen-free conditions with ad libitum access to food and water. The experiments were performed in accordance with the CCAC guidelines and approved by the ethical committee of the Plateforme d'Evaluation Préclinique of Gustave Roussy. The animals were allocated to experimental groups to achieve similar mean tumor volumes in each group on day 0 of treatment. Female C57Bl/6 OlaHsd mice were purchased from Envigo and nude (athymic) mice were purchased from the animal facility of Gustave Roussy. At 6–8 weeks of age, the mice were injected subcutaneously into the flank with 8×10^5 BP cells in 100 µl PBS. After 6 d and after the tumors had reached an average volume of ~100 mm^3, the mice received an intraperitoneal injection of silvestrol (0.5 mg per kg body weight) daily. Silvestrol was dissolved in DMSO to generate a 0.03 mg ml^{-1} stock solution and then diluted in PBS containing 5% Kolliphor (Sigma). Tumor growth was monitored twice a week in two dimensions using a digital caliper. The tumor volumes were calculated using the following ellipsoid volume formula: $V=(L\times W^2)/2$, where L is the length and W is the width.

For the CD8 immunofluorescence, tumors were excised, sectioned and fixed in methanol. CD8 (1:100; Ebioscience, 50-0081-82) immunostaining was conducted.

PD-L1 and STAT1 overexpression. The BP and A375 cells were infected with lentiviruses encoding murine PD-L1 coupled with GFP (Origene) and human STAT1 coupled with GFP (Origene), respectively, at a multiplicity of infection (MOI) of 0.5. Subsequently, 72 h after the infection, cell sorting was performed to isolate GFP^+ cells using a FACSARIA III cell sorter (BD Biosciences).

Statistical analysis. For statistical analysis, we used GraphPad Prism software v.7.04. Figure legends specify the statistical analysis used and define error bars. For microarray analysis, the statistical analysis performed is described in the corresponding section of the Methods.

Reporting Summary. Further information on experimental design is available in the Nature Research Reporting Summary linked to this article.

Data availability

The data sets generated for this study can be accessed at GEO (GSE118521). Uncropped immunoblots are available in Supplementary Fig. 13, data obtained from human tumor samples in Supplementary Table 4 and primer sequences in Supplementary Table 5.

References

53. Botton, T. et al. In vitro and in vivo anti-melanoma effects of ciglitazone. *J. Invest. Dermatol.* **129**, 1208–1218 (2009).
54. Tichet, M. et al. Tumour-derived SPARC drives vascular permeability and extravasation through endothelial VCAM1 signalling to promote metastasis. *Nat. Commun.* **6**, 6993 (2015).
55. Tsukiyama-Kohara, K. et al. Adipose tissue reduction in mice lacking the translational inhibitor 4E-BP1. *Nat. Med.* **7**, 1128–1132 (2001).
56. Banko, J. L. et al. The translation repressor 4E-BP2 is critical for eIF4F complex formation, synaptic plasticity, and memory in the hippocampus. *J. Neurosci.* **25**, 9581–9590 (2005).
57. Yajima, I. et al. Spatiotemporal gene control by the Cre-ERT2 system in melanocytes. *Genesis* **44**, 34–43 (2006).
58. Dorard, C. et al. RAF proteins exert both specific and compensatory functions during tumour progression of NRAS-driven melanoma. *Nat. Commun.* **8**, 15262 (2017).

nature research

Corresponding author(s): Stéphan VAGNER, Caroline ROBERT

☐ Initial submission ☐ Revised version ☒ Final submission

Life Sciences Reporting Summary

Nature Research wishes to improve the reproducibility of the work that we publish. This form is intended for publication with all accepted life science papers and provides structure for consistency and transparency in reporting. Every life science submission will use this form; some list items might not apply to an individual manuscript, but all fields must be completed for clarity.

For further information on the points included in this form, see Reporting Life Sciences Research. For further information on Nature Research policies, including our data availability policy, see Authors & Referees and the Editorial Policy Checklist.

Experimental design

1. Sample size

Describe how sample size was determined.

For animal studies, sample size was defined on the basis of past experience on cancer in order to detect the biggest difference possible between the groups.

2. Data exclusions

Describe any data exclusions.

no excluded data

3. Replication

Describe whether the experimental findings were reliably reproduced.

All attempts at replication of in-vitro experiments were successful

4. Randomization

Describe how samples/organisms/participants were allocated into experimental groups.

For all in vivo experiments mice were randomized the day after tumor cells injection.

5. Blinding

Describe whether the investigators were blinded to group allocation during data collection and/or analysis.

experiments were not done blindly because it was the same persons who performed the experiments and analysed the data

Note: all studies involving animals and/or human research participants must disclose whether blinding and randomization were used.

6. Statistical parameters

For all figures and tables that use statistical methods, confirm that the following items are present in relevant figure legends (or in the Methods section if additional space is needed).

n/a	Confirmed	
☐	☒	The exact sample size (*n*) for each experimental group/condition, given as a discrete number and unit of measurement (animals, litters, cultures, etc.)
☐	☒	A description of how samples were collected, noting whether measurements were taken from distinct samples or whether the same sample was measured repeatedly
☐	☒	A statement indicating how many times each experiment was replicated
☐	☒	The statistical test(s) used and whether they are one- or two-sided (note: only common tests should be described solely by name; more complex techniques should be described in the Methods section)
☒	☐	A description of any assumptions or corrections, such as an adjustment for multiple comparisons
☐	☒	The test results (e.g. *P* values) given as exact values whenever possible and with confidence intervals noted
☐	☒	A clear description of statistics including central tendency (e.g. median, mean) and variation (e.g. standard deviation, interquartile range)
☐	☒	Clearly defined error bars

See the web collection on statistics for biologists for further resources and guidance.

Software

Policy information about availability of computer code

7. Software

Describe the software used to analyze the data in this study.	We have used GraphPad for basic statistics, FlowJo for cytometry data analysis, Compass for microfluidic western blot analysis, Image J for immunohistochemistry and immunofluorescence analysis, MORPHEUS for the generation of the heatmap, R and Xtail software for the microarry experiment and the translation efficency analysis

For manuscripts utilizing custom algorithms or software that are central to the paper but not yet described in the published literature, software must be made available to editors and reviewers upon request. We strongly encourage code deposition in a community repository (e.g. GitHub). *Nature Methods* guidance for providing algorithms and software for publication provides further information on this topic.

Materials and reagents

Policy information about availability of materials

8. Materials availability

Indicate whether there are restrictions on availability of unique materials or if these materials are only available for distribution by a for-profit company.	All materials used in this study are available from standard commercial sources except FL3 and PhenDC3. To obtain FL3 or PhenDC3 please contact L. Désaubry and M.P. Teulade-Fichou respectively.

9. Antibodies

Describe the antibodies used and how they were validated for use in the system under study (i.e. assay and species).	From BioLegend: human PD-L1 (catalogue no. 329708), mouse PD-L1 (catalogue no. 124312) and mouse CD45 (catalogue no. 103128). An isotype was used as a nonspecific control according to the datasheet supplied with each antibody. From Cell Signaling Technologies: eIF4G (catalogue no. 2498), 4EBP1 (catalogue no. 9644), 4EBP2 (catalogue no. 2445), eIF4E (catalogue no. 2067), eIF4A1 (catalogue no. 2490), and STAT1 (catalogue no. 9179). From Santa Cruz Biotechnology : the antibody specific for HSP90 (catalogue no. sc-13119), c-myc (clone 9E10, catalogue no. sc-40), vinculin (clone H-10, catalogue no. sc-25336). The antibody specific for GAPDH (catalogue no. MAB374) was purchased from Millipore. The antibody specific to β-actin (catalogue no. A5060) was purchased from Sigma. The antibody specific to IRF-7 was purchased from abcam (catalogue no. 109255). The antibody specific to MHC class I (catalogue no. MAS-16562) was purchased from Thermo. The antibody anti-mouse (catalogue no. 042-205) and anti-rabbit (catalogue no. 043-426) coupled to HRP was purchased from Biotechne.

10. Eukaryotic cell lines

a. State the source of each eukaryotic cell line used.	The following cell lines were used: A375, WM793, SKMel10, A2058, SKMel28, SKMel2, MCF7, A549, HT29 and 4T1 cell lines. BRAFV600E PTEN knockout melanoma cells derived from Tyr:CreERT2/0;BrafCA; Ptenlox/lox mice established by J. Wargo team. BRAFV600E melanoma cells derived from Braf+/LSL-V600E;Tyr::CreERT2/o mice and BRAFV600E 4EBP1/2 knockout melanoma cells derived from Braf+/LSL-V600E;Tyr::CreERT2/o 4ebp1 4ebp2 knockout mice established by A. Eychène team.
b. Describe the method of cell line authentication used.	A375, A2058, SKMel28 SKMel2 and 4T1 cells were received from ATCC just before use. SKMel10, WM793, MCF7, A549 and HT29 cells were authenticated by checking morphology by microscopy.
c. Report whether the cell lines were tested for mycoplasma contamination.	Cell lines are tested each month for mycoplasma contamination and are used for experiments only when they are negative
d. If any of the cell lines used are listed in the database of commonly misidentified cell lines maintained by ICLAC, provide a scientific rationale for their use.	no commonly misidentified cell lines were used

Animals and human research participants

Policy information about studies involving animals; when reporting animal research, follow the ARRIVE guidelines

11. Description of research animals

Provide details on animals and/or animal-derived materials used in the study.

6–8 weeks females C57BL/6J Ola/Hsd and Nude (athymic) mice were purchased from Envigo and from the animal facility of Gustave Roussy respectively.
The 4ebp1–/– , 4ebp2–/– , Braf+/LSL-V600E and Tyr::CreERT2/o mice have been previously described.

Policy information about studies involving human research participants

12. Description of human research participants

Describe the covariate-relevant population characteristics of the human research participants.

Human peripheral mononuclear cells (PBMCs) were isolated from peripheral blood of healthy donors of "Etablissement Francais du Sang".
Tumors samples come from the biobank of Gustave Roussy. The characteristics of the patients are availables in the supplementary table 4.